NTNU – Trondheim
Norwegian University of
Science and Technology

State and Parameter Identification Applied to Dual Gradient Drilling with Water Based Mud

Simon Haukanes

Master of Science in Cybernetics and Robotics
Submission date: June 2015
Supervisor: Ole Morten Aamo, ITK
Co-supervisor: Espen Hauge, Statoil

Norwegian University of Science and Technology
Department of Engineering Cybernetics

Problem Description

Title:
State and Parameter Identification Applied to Dual Gradient Drilling with Water Based Mud.

Deepwater drilling is challenging business. After Macondo, the industry has been stimulated to come up with new solutions improving safety. The past few years, the costs of drilling wells have increased significantly while the oil price has dropped. To stay in business and to be able to drill planned wells in a profitable manner, both safety and efficiency have to be improved. Managed Pressure Drilling (MPD) for floaters is a technology, where rig time spent on handling wellbore instabilities, such as kicks and losses, can be reduced. Accurate control of the downhole pressures enables drilling through narrow drilling windows with reduced risk of taking an influx or going on varying degrees of losses.

After gaining operational experience with dual gradient drilling (DGD), field data has become available. This field data gives the opportunity to validate mathematical models and estimate unknown parameters. Once a verified model has been established, it can be used to experiment with controller design and tuning. This will ease controller tuning offshore, which in turn saves valuable rig time.

Goal:
Find a mathematical model of a DGD system and estimate its unknown parameters from field data.

Subtasks:

- Find a suitable model for the DGD system.
- Find sensitivities of parameters and determine how to find each of the parameters.
- Estimate unknown parameters which do not rely on dynamics.
- Estimate unknown parameters for a linearized version of the model.
- Estimate unknown parameters of the non-linear model.
- Possible augmentation of the model.

Summary

There is a continuous search for new reserves in the oil and gas industry. Most of the larger fields that are accessible with conventional drilling technology have been drilled. The remaining fields typically contain less oil and gas, are harder to drill and located at significant depths. The costs of drilling wells have increased while the oil price has dropped. It is therefore a strong demand for drilling technologies able to drill where conventional drilling cannot be used, while still being cost and time efficient. In addition, after the blowout in the Gulf of Mexico, the industry has been challenged to develop new solutions improving safety. As a response to increased demands, solutions with a higher degree of automation, improving pressure control have been developed, and are referred to as Managed Pressure Drilling. A sub technology in this category is Dual Gradient Drilling.

Statoil ASA uses this technology at one of their offshore installations, and after gaining operational experience, field data has become available. This field data gives the opportunity to validate mathematical models and estimate unknown parameters. Once a verified model has been established, it can be used to experiment with controller design and tuning. This will ease controller tuning offshore, which in turn saves valuable rig time.

In this thesis, a fit-for-purpose mathematical model for a Dual Gradient Drilling system with partially filled riser is derived. Using the available field data, unknown parameters related to the mud circulation part of the system is identified. The model is also augmented to account for the presence of the U-tubing effect. A steady state friction model was found sufficient to describe the frictional losses, and a subsea pump model was obtained by optimization. The presence of U-tubing was found when ramping down the booster pump. Due to the lack of measurements and in-depth system knowledge, a complicated model was discarded in favor of adding simplified dynamics to the booster pump. The simple model successfully compensated for U-tubing. Through simulation the derived model, with identified parameters, was found to be able to reproduce the field data in a satisfactory manner with only small deviations during U-tubing.

Sammendrag

Det er et stadig pågående søk etter nye reserver i olje og gass industrien. De fleste større felt, som er tilgjengelige med konvensjonell boreteknologi, har allerede blitt utforsket. Gjenstående felt inneholder mindre olje og gass, er vanskelige å bore, og ofte lokalisert på store havdyp. Kostnadene ved boring har økt, samtidig som oljeprisene synker. Det er derfor sterk etterspørsel i industrien for boreteknologier som muliggjør boring hvor konvensjonell ikke strekker til, og som samtidig er tids- og kostnadseffektive. Samtidig, etter ulykken i Mexicogolfen har industrien blitt utfordret til å utvikle metoder som øker sikkerheten. Som en respons på dette har nye, mer automatiserte boremetoder som forbedrer trykkontroll blitt utviklet. Disse metodene kalles trykkstyrt boring. En av teknologiene i denne kategorien er "Dual Gradient" boring.

Statoil bruker denne teknologien på en av sine installasjoner, og har fått driftserfaring, slik at feltdata nå er tilgjengelig. Disse feltdataene gjør det mulig å validere matematiske modeller og estimere ukjente parametere. Når en modell er tilpasset og verifisert, kan den brukes for simulering i tillegg til design og innstilling av regulatorer. Dette gjør regulatorinstilling på boreriggen offshore enklere, og verdifull rigtid kan dermed spares.

I denne oppgaven utledes en matematisk modell for et "Dual Gradient" boresystem med delvis fylt stigrør. Ved hjelp av feltdata ble ukjente parametre i modellen estimert. Modellen ble også utvidet for å ta høyde for "U-tube" effekten. En stasjonær friksjonsmodell ble funnet tilstrekkelig for beskrive trykktap som følge av friksjon. Videre ble en modell for undervannspumpen som returnerer borevæske funnert ved optimalisering. U-tubing ble med hell tatt høyde for ved å legge til ekstra dynamikk på "booster" pumpen. På grunn av manglende måledata ble en mer omfattende U-tube modell forkastet. Gjennom simulering ble det vist at modellen med estimerte parametre klarte å gjennskape måledata presist, med lite avvik i stigrørnivå.

Preface

This thesis has been written during the final semester of my Master of Technology studies in Engineering Cybernetics at the Norwegian University of Science and Technology (NTNU).
I would like to thank my supervisor Professor Ole Morten Aamo at NTNU for his guidance and help. I would also like to thank my co-supervisor Espen Hauge at Statoil ASA for presenting the project, providing field data and answering questions throughout the work. Also, thanks to the fellow students in G238 for the good times in the office.

Simon Haukanes
Trondheim, June 2015

Table of Contents

List of Tables

List of Figures

Abbreviations

MPD Managed Pressure Drilling

DGD Dual Gradient Drilling

BOP Blow Out Preventer

ODE Ordinary Differential Equation

PDP Positive Displacement Pump

MSE Mean Squared Error

LS Least Squares

RKB Rotary Kelly Bushing

PT Pressure Transmitter

FT Flow Transmitter

CV Controlled Variable

DAE Differential Algebraic Equation

Chapter 1

Background

This introductory chapter contains the general motivation for the work done, along with the main goals. Additionally, a brief introduction to drilling is presented. More in-depth information regarding general offshore drilling and different technologies can be found in i.e. Wenaas (2014).

1.1 Motivation and Introduction to Drilling

The demand for oil and gas is increasing and there is a continuous search for new reserves. Most of the larger fields that are accessible with conventional drilling technology have been drilled, and the remaining fields typically contain less oil and gas, are harder to drill and located at significant depths. A common expression states that the days of so-called ”easy oil” is over, and the oil companies have been forced into more remote and challenging environments. Consequently, over the past few years the costs of drilling wells have increased while the oil price has dropped. Also, after the Macondo blowout in the Gulf of Mexico, the industry has been challenged to develop new solutions improving safety. To stay in business and to be able to drill planned wells in a profitable manner, both safety and efficiency have to be improved. It is therefore a strong demand for drilling technologies able to drill where conventional drilling cannot be used, while still being cost and time efficient.

As an introduction to drilling, consider the setup in figure (1.1). When drilling a new well, a blowout preventer (BOP) is placed on the seabed and a wide pipe called the riser is lowered from the rig and attached to the BOP. Further, the drill string with attached drill bit is lowered through the BOP. At the top of the derrick the drill string is attached to the top drive, which rotates the drill string. As drilling progresses, the drill string needs to be extended, and a new section of drill string pipe is connected, referred to as a pipe connection. During drilling of the well, cuttings needs to be transported out of the bore-hole. This is done by pumping a drilling fluid called mud through the drill string. The mud flows through the drill bit, and up the annulus around the drill string, carrying the cuttings

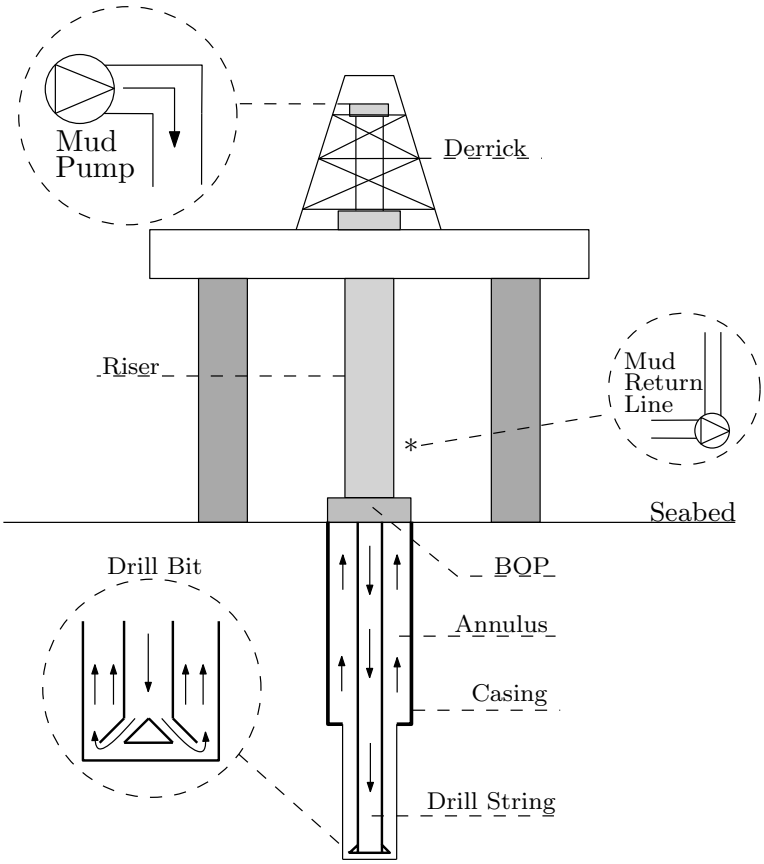

Figure 1.1: Offshore drilling platform. Mud flows from the main pump, through the drill string, drill bit and back up through the annulus and riser. For a DGD system, a dedicated mud-return line is used instead of returning mud at the top of the riser. Figure inspired by Stamnes (2011).

before it exits the riser and is recycled topside. The mud needs sufficiently high viscosity to carry cuttings, and at the same time sufficiently high density to meet the well pressure conditions. Typically the mud is water or oil based.

1.1.1 Pressure Control

Control of downhole pressure is a crucial part of drilling. The annular pressure profile must be kept within certain bounds. That is, above the pore pressure and collapse pressure, and below the fracture pressure of the bore hole. The downhole pressure is governed by the following pressure boundaries

$$P_{\text{pore}} \text{ or } P_{\text{collapse}} < P_{\text{downhole}} < P_{\text{fracture}}$$

where whichever one of the pore and collapse pressure with the highest value determines the lower bound. If the pressure decreases below the pore pressure, formation fluids can

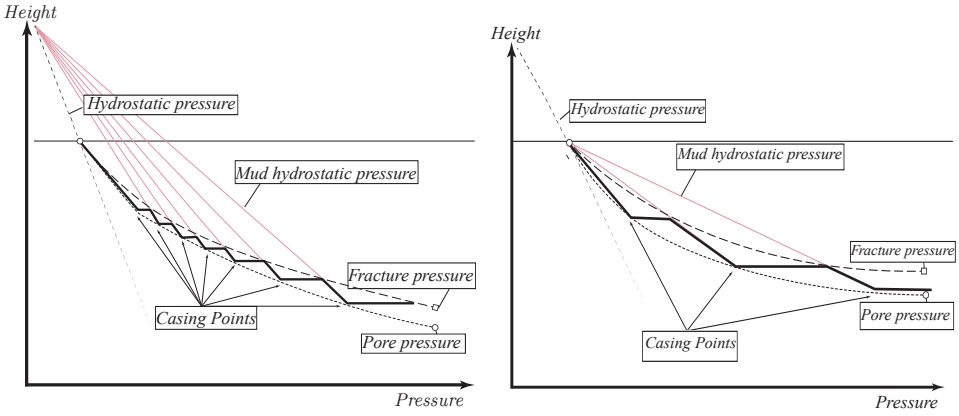

(a) Pressure profile and casing point for conventional drilling.

(b) Pressure profile and casing points for dual gradient drilling.

Figure 1.2: Pressure versus depth graphs. Figures from Fossum (2013)

potentially flow into the annulus. This is called a kick and if not detected, and dealt with properly, it can cause an uncontrolled blowout with fatal consequences. If the pressure falls below the collapse pressure, the well can collapse and the drill sting can be stuck downhole. On the other hand, if the annular pressure exceeds the fracture pressure, mud can be lost into the formation and damage the permeability (a measure of the ability of fluids to flow trough rock) properties of the reservoir. In conventional drilling, pressure control is done by circulating in new mud with different density when the pressure profile needs to be changed. Figure (1.2a) shows a typical pressure versus depth graph for a offshore well. When the drillbit reaches the depths labeled ”casing points”, the pressure is close to the pore/ collapse pressure. A casing (steel cylinders) must be placed in the well to isolate the well from the formation and a heavier mud is needed to drill further. This is a slow and inefficient process, and wells with tight pressure margins are practically ”undrillable”. As a response to increased demands, drilling solutions improving pressure control have been developed, and are refereed to as Managed Pressure Drilling (MPD). MPD is an adaptive drilling process used to precisely control the pressure profile throughout the well bore, Malloy et al. (2009). Multiple sub-methods exits and the most common methods uses control of back pressure by using a pressurized mud return system or a submerged mud return pump. Combined with increased interest and use of automatic control, Godhavn et al. (2011), these drilling technologies have made it possible to drill previously non-drillabe wells, and at the same time increasing efficiency and safety overall.

One of these methods is called Dual Gradient Drilling (DGD). In the early 1990’s there were several deepwater oil discoveries in the Gulf of Mexico, which led to an increased interest in drilling technologies suited for deepwater drilling. The goal with DGD was ultimately to eliminate the riser, and the concept was thus originally called ”Riserless Drilling”, Smith et al. (2001). Ultimately, the driving factor to develop DGD became the need of managing narrow pressure margins in deepwater wells, and reduce the number

of casing points. DGD methods are usually characterized by a partially mud-filled riser, topped with a lighter fluid. Often the top gradient is air, but other fluids can be used. To control the mud level, DGD uses a separate mud return line to the surface. A pressure versus depth graph for a DGD system is shown in figure (1.2b). By lowering the mud-line in the riser, higher density mud can be used and longer sections can be drilled at the time. As seen the number of casing points are decreased significantly. There exists a multiple sub-technologies in the DGD category. The one in focus of this thesis is called ”Controlled Mud Level”. The hydrostatic pressure in the well is controlled by adjusting the mud level in the riser, where the top gradient is air. The level is adjusted using an automatic controlled subsea pump as seen in figure (1.1), where the mud return line is marked with an asterisk.

Statoil ASA uses this technology at one of their offshore installations, and after gaining operational experience field data has become available. This field data gives the opportunity to validate mathematical models and estimate unknown parameters. Once a verified model has been established, it can be used to experiment with controller design and tuning. This will ease controller tuning offshore, which in turn saves valuable rig time, and thus increases time and cost efficiency.

1.2 Previous Work on DGD

A lot of research has been done in the area of MPD technologies. In a case study, Wenaas (2014) presents the main development of the MPD, including DGD technology. A lot of effort have been put into the issue of estimating the bottom hole pressure, base on topside measurements, e.g. in Stamnes et al. (2008). Different approaches to pressure control with various adaptive techniques can be found in Zhou et al. (2008a) and Zhou et al. (2008b). Central in the models development is the simplified hydraulic model for MPD system presented in Kaasa et al. (2012) (originally published in an earlier internal paper). Further, issues on the heave problem, that is pressure fluctuations in the well due to vertical rig motion, have been researched. Disturbance rejection strategies are the topic in e.g. Landet (2011) and Anfinsen and Aamo (2013). Breyholtz et al. (2011) extends the model presented in Kaasa et al. (2012), and presents a modified version for a DGD system, which is used to implement a model predictive controller that coordinates control of the subsea pump and topside equipment. In Stamnes et al. (2012) the DGD model is further extended to include two fluids in the well, e.g. when changing mud. The U-tubing problem in DGD is investigated in Anfinsen (2012). In recent years multiple DGD variations have been developed and tested, e.g. versions of the ”Riserless Mud Recovery” technology, described in Stave (2014).

1.3 Scope and Emphasis

The main goal of this thesis is firstly to derive a fit-for-purpose mathematical model for the DGD system that is suitable for system identification. The model is derived for the full DGD system. However, the focus of the identification is on the mud circulation sys-

tem. The unknown parameter in the model is estimated using field data provided by Statoil ASA. The system identification is done by a ”divide and conquer” approach, where different parts are isolated, for parameter estimation and comparison to available measurements. Work is also put into revising the model, in order to capture different dynamics found during the identification procedure.

1.4 Outline of Thesis

This thesis is outlined in the following way: **Chapter 2** contains the derivation of the mathematical model for the DGD system. A complete fit for purpose model is presented. **Chapter 3** is a comprehensive chapter, where everything related to system identification is found. A brief sensitivity analysis and a short analysis of the available data is found here. Also, both parameters related and not related to dynamics are estimated. A model augmentation is also done to include the U-tubing effect. In **Chapter 4** a model verification is done. That is, the complete identified model is compared to the available measurement data. Lastly, the conclusion and suggestions for further work are found in **Chapter 5**.

Chapter 2

Modeling

A dynamic model for a typical DGD system will be derived in this chapter. A lot of work has been done on mathematical modeling of drilling systems, and advanced hydraulic models have been developed, that capture all aspects of drilling dynamics. These models are able to reproduce specific drilling effects with a high degree of detail. However, the model accuracy is limited by the least accurate term. In order to maintain high model accuracy several parameters, which often depend on temperature, friction coefficient etc., must be calibrated. In practice these parameters must be estimated using topside measurements, and if available downhole measurements. The available data contains, in most cases, insufficient information to properly estimate all parameters in an advanced hydraulic model. Hence, as the well conditions are uncertain and inhomogeneous, much of the advanced modeling does not improve the overall model accuracy without additional measurements along the well.

The main objective of the model is to be used for identifying unknown parameters, and further to use when designing and tuning control systems. Both of which are easier using a simplified model. A control system is only able to compensate for changes in a particular frequency range, referred to as the bandwidth of the closed-loop system. In this case, the achievable bandwidth is determined by dynamic response of the subsea pump, which is the main source of control in the DGD system. The control system is not able to compensate for high frequency dynamics, and consequently high frequency components in the model are undesirable. Therefore, from a control perspective, the goal is to remove complexity, without sacrificing dynamics in the frequency range of interest. In addition, from a system identification perspective, a model where all the parameters can be obtained by available data is needed.

Multiple papers have been written on the topic of simplified mathematical models for drilling systems. Central in the model development is the simplified hydraulic model for a back pressure MPD system, presented in Kaasa et al. (2011) (originally presented in a earlier internal paper). This model is also revisited in Stamnes (2011), where it is used as

a basis for developing an adaptive observer for down hole pressure. The Kaasa model is based on the traditional MPD setup with a closed off annulus and a topside control valve. To include the DGD setup with a partially filled riser and a separate mud return line, the model must be augmented. This is done in Breyholtz et al. (2011) where a model modified for a DGD system is presented. This model is revised and further extended in Stamnes et al. (2012) where the scenario with two fluids in the well is included. Also, a realistic model of the subsea pump is suggested. The same model is used in Anfinsen (2012) with main efforts on modeling the U-tubing effects. The following model derivation is based on the original model in Kaasa et al. (2011), with additional information about the derivation is included based on Stamnes (2011), Stamnes et al. (2012) and Anfinsen (2012), and further extended for the purposes in this thesis.

2.1 Fit-for-purpose modeling

For control and system identification purposes the objective is to develop an as simple model as possible, by removing complexity that does not affect the main system dynamics. Additionally the model should be optimized for utilizing existing measurements in order to estimate the unknown system parameters. Kaasa et al. (2011) identifies the main simplifications applied to obtain a fit-for-purpose model as 1) Neglecting dynamics which is much faster than the bandwidth of the control system. 2) Neglecting slow dynamics. Slowly changing system properties are easier handled by feedback in the control system or parameter estimation, than to include them in the model. 3) Lump together parameters which is not possible to distinguish with the available measurements.

2.1.1 Assumptions

For the model derivation it is assumed that the drilling fluid can be treated as a viscous fluid, which means that the flow is completely described using the fundamental laws of fluid mechanics

- *Conservation of Mass:* Continuity equation (mass balance)
- *Conservation of Momentum:* Newtons second law of motion (force balance)
- *Conservation of Energy:* First law of thermodynamics (energy balance)
- *Fluid viscosity:* The viscosity is a function of pressure and temperature
- *Equation of state:* The density is a function of pressure and temperature

Additionally, some basic assumptions are made prior to the model derivation. Firstly, it is assumed that the flow can be treated as one-dimensional along the flow path. That is, time-averaging fluctuations due to turbulence. The flow is also considered to be radially homogeneous such that properties over the cross-section can be averaged. Additionally, the assumption of incompressible flow is made such that the time variance of the dentistry in the momentum equation can be neglected. Lastly it is assumed that the time variance of the viscosity is negligible in the momentum equation. Some additional assumptions are made during the model derivation and are stated just prior to their use.

2.2 Pressure Dynamics

For a one-dimensional flow through a control volume V, the differential continuity equation, which describes the conservation of mass in V, is given as

$$\frac{\partial \rho}{\partial t} + \frac{\partial}{\partial x}(\rho v) = 0 \tag{2.1}$$

where v is the velocity of the flow, and x is the spatial variable along the flow path. With average density $\bar{\rho}$ and with well defined inlets and outlets, the equation for mass conservation can be found on differential form by integrating 2.1 over V, yielding

$$\frac{d}{dt}m = \sum \bar{\rho}_{in} q_{in} - \sum \bar{\rho}_{out} q_{out}. \tag{2.2}$$

where $\rho_{in} q_{in} = m_{in}$ and $\rho_{out} q_{out} = m_{in}$ is the mass flow in and out of the control volume. The average density $\bar{\rho}$ in V is defined as

$$\bar{\rho} = \frac{1}{V} \int_0^L \rho(x) A(x) dx$$

where L is the length of the volume in x-direction and $A(x)$ is the cross-sectional area of the pipe.
Equation (2.2) is further rewritten in terms of density and volume, yielding

$$\frac{d}{dt}(\bar{\rho} V) = V \dot{\bar{\rho}} + \bar{\rho} \dot{V} = \sum \bar{\rho}_{in} q_{in} - \sum \bar{\rho}_{out} q_{out}. \tag{2.3}$$

In order to get pressure as the main variable, equation (2.3) is rewritten using a simplified version of the equation of state from Egeland and Gravdahl (2002) on the form

$$\frac{d\rho}{\rho} = \frac{dp}{\beta}. \tag{2.4}$$

where β is the bulk modulus, defined in Merritt (1967) as

$$\beta = -V_0 \left. \frac{\partial p}{\partial V} \right|_{T_0} \tag{2.5}$$

resulting in the general expression for the pressure dynamics

$$\bar{\rho} \frac{V}{\beta} \frac{d\bar{p}}{dt} + \bar{\rho} \frac{dV}{dt} = \sum \rho_{in} q_{in} - \sum \rho_{out} q_{out}. \tag{2.6}$$

It is further assumed that the change in average pressure with respect to time is the same as the change in pressure anywhere in the control volume, hence $\dot{\bar{p}} = \dot{p}$. Additionally, it is assumed that for all the considered control volumes, the density of the fluid pumped into the control volume is equal to the average density in the volume and the fluid leaving the volume $\bar{\rho} = \rho_{in} = \rho_{out} = \rho$, resulting in

$$\frac{V}{\beta} \dot{p} + \dot{V} = \sum q_{in} - \sum q_{out} \tag{2.7}$$

2.2.1 Equation of State

The bulk modulus β relates to the stiffness of the fluid, and is the reciprocal of the compressibility of the liquid (Kaasa et al. (2011)). It is the dominant property when determining the system dynamics, as is characterizes the pressure transients in the system. Pressure transients of a well is typically in the range of seconds to minutes, which is within the bandwidth of the control system.
The general expression for the equation of state is on the form

$$\rho = \rho(p, T)$$

which states that the density is a function of pressure and temperature. However, as the dependency is small for liquids, it is common to use the linearized equation of state. In general the linearized version is said to be accurate for most drilling fluids within normal operating conditions (Stamnes (2011)). However, as demonstrated by Isambourg et al. (1996) in laboratory tests, density changes can be significant particularly for High- Pressure High-Temperature wells, where the temperature range is large. To capture the effect of temperature transients, the full linearized equation of state can be used in the model derivation

$$d\rho = \frac{\rho}{\beta} d\rho - \rho \alpha dT$$

where α is the expansion coefficient for the liquid.

The simplified linearized version used in (2.4), neglects temperature dependency entirely. It is assumed for the purposes of this model that the relatively slow, if any, temperature transients and are more efficiently handled by feedback in the control system and hence neglected.

2.2.2 Advanced Hydraulic Modeling

Assuming the cross sectional area of the flow path is piecewise constant $A(x)$, the equation of continuity (2.1) can be rewritten as

$$\frac{\partial p(x,t)}{\partial t} = -\frac{\beta}{A} \frac{\partial q(x,t)}{\partial x} \tag{2.8}$$

which is commonly used to describe pressure dynamics advanced in hydraulic models with differential control volumes together with

$$\frac{\partial q(x,t)}{\partial t} = -\frac{A}{\rho} \frac{\partial p(x,t)}{\partial x} - \frac{F}{\rho} + Agcos(\theta). \tag{2.9}$$

describing the flow. These are the equations describing a hydraulic transmission line and are found e.g. in Egeland and Gravdahl (2002).
Landet (2011) presents a well model based on this model, which he discretize, using the

finite volume method. This results in a set of ordinary differential equations (ODE's), describing the pressure and flow at multiple positions or nodes in the control volumes, as seen in figure (2.1), that is the drill string, well, and annulus. This is done to accurately capture the pressure fluctuations caused by heave motion that occur when drilling from a floating rig.

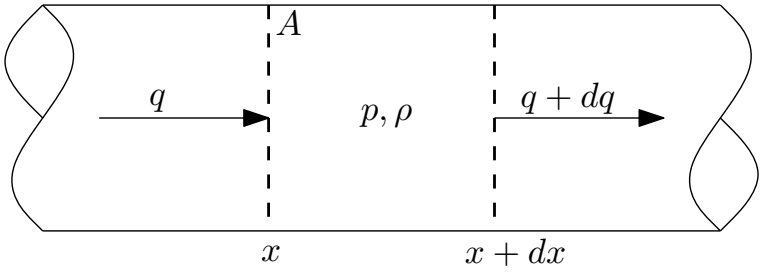

Figure 2.1: Volume element for a hydraulic transmission line

In the derivation of the mass balance for a volume V for use in this thesis it is assumed that the pressure are the same over the volume, and that multiple pressure nodes in the V, is unnecessary. This means that the pressure $p = p(t)$ is a function of time only. The main pressure transient property, β, is reflected in the pressure along the entire flow path, and the pressure at any point in the well can be approximated by the average pressure. Pressure changes propagate with the speed of sound, which is $c = 1484$ m/s in water. For a pipe with length L, the time for a pressure change to propagate is stated in Egeland and Gravdahl (2002) as $T = L/c$. For a pipe with length of 500 meters, the pressure differences in the volume will disappear after about 0.3 seconds. This is usually much faster that the bandwidth of the control system and is thus neglected in the model.

2.2.3 Drill string and booster line

When considering the drill string, that is the control volume from the mud pump to the drill bit, the pressure dynamics (2.7) is given as

$$\frac{V_d}{\beta_d}\frac{dp_p}{dt} = q_p - q_{bit} \tag{2.10}$$

where the subscript $\bullet_d$ denotes the drill string and V_d, β_d, q_p and q_{bit} are the drill string volume, the effective bulk modulus, mud pump flow and flow through the drill bit respectively. It is here assumed that the drill string volume is constant during normal drilling operations, such that its time derivative, $\dot{V}_d$, is zero.

Similarly, when considering the flow from the booster pump to the booster line outlet, the pressure dynamics are given as

$$\frac{V_b}{\beta_b}\frac{dp_b}{dt} = q_{boost} - q_{bo} \tag{2.11}$$

where the subscript $\bullet_b$ denotes the booster line and V_b, β_b, q_{boost} and q_{bo} are the booster line volume, the effective bulk modulus, booster pump flow and flow through the booster line outlet respectively.

2.2.4 Riser

In the DGD system the riser is open to the atmosphere. Consequently, compressibility effects caused by pressure variations in the riser and annulus are negligible. With the simplification $\frac{dp_r}{dt} = 0$, where the subscript $\bullet_r$ denotes the riser, equation 2.7 is reduced to the volume balance

$$\dot{V}_r = \sum q_{in} - \sum q_{out}.$$

With the defined inlet and outlet flows, the total fluid volume in the riser and annulus is given as

$$\dot{V}_r = q_{bit} + q_{boost} + q_{tf} + q_{res} - q_{ssp} \tag{2.12}$$

where q_{boost} is a flow entering the bottom of the riser through the booster line, q_{res} is an influx flow from the well, q_{tf} is the top-fill flow entering at the top of the riser, and q_{ssp} is the flow leaving the riser through the sub sea pump. Well influx is disregarded in the model, and it is further assumed that $q_{res} = 0$.

The fluid volume in the annulus and riser is given as $V_r = V_{r,0} - A_r(h_r)h_r$ where $V_{r,0}$ is the constant total volume and h_r is the fluid level in the riser, defined downwards from the top of the riser.Using this, equation (2.12) can be written as

$$-\frac{d}{dt}\left(A_a(h_r)h_r\right) = q_{bit} + q_{boost} + q_{tf} - q_{ssp}. \tag{2.13}$$

Assuming that the riser cross-sectional area, A_r, is constant in the range where the riser level varies, the following expression for the riser level is found

$$\dot{h}_r = \frac{1}{A_r}\left(q_{ssp} - q_{bit} - q_{boost} - q_{tf}\right). \tag{2.14}$$

Similarly, for the case where the rig-pump and booster-pump are disconnected and open to the atmosphere, the level dynamics are given as

$$\dot{x}_d = \frac{1}{A_d}(q_{bit} - q_p)$$

for the drill-string and

$$\dot{x}_b = \frac{1}{A_b}(q_{bo} - q_{boost})$$

for the booster line.

2.3 Flow Dynamics

The basis for the flow dynamics for a differential control volume is the momentum balance, see e.g. White (2011),

$$\sum \mathbf{F} = \rho \frac{d\mathbf{V}}{dt} dxdydz \tag{2.15}$$

where $\sum \mathbf{F}$ is the sum of forces acting on the differential volume, and $\mathbf{V}$ is the velocity vector. For the case of one- dimensional flow in x-direction, (2.15) reduces to

$$\sum F_x = \rho \frac{dv}{dt} A(x) dx \tag{2.16}$$

where v is the velocity in x-direction and $A(x)$ is the cross sectional area. The forces acting on the control volume are external fields such as gravity and surface forces such as hydrostatic pressure gradients and frictional forces. The basic one- dimensional differential momentum equation considering these forces is given as

$$\rho \frac{\partial v}{\partial t} = -\frac{\partial p}{\partial x} - \frac{\partial \tau}{\partial x} + \rho g \cos(\phi) \tag{2.17}$$

where τ is the viscous forces, and ϕ is the angle of the flow path inclination. τ is a lumped term including all frictional losses such as viscous effects, turbulence and flow restrictions. Typically the friction term is a function of flow rate and is in general on the form

$$\tau = \tau(q, \mu)$$

where μ is the fluid viscosity. By using an accurate friction model, much of the loss in accuracy due to the basic assumptions can be recovered. Examples of frictional dynamics is gelling. External inputs such as drill pipe rotation can also be included to account for the effect of swirl flow. By including such friction models, the steady state and transient accuracy can be significantly improved (Kaasa et al. (2011)).

In terms of flow rate q, using $u = \frac{q}{A(x)}$, equation (2.17) can be rewritten as

$$\frac{\rho}{A} \frac{\partial q}{\partial t} = -\frac{\partial p}{\partial x} - \frac{\partial \tau}{\partial x} + \rho g \cos(\phi). \tag{2.18}$$

An equation describing the average flow dynamics in the control volume is found by assuming the fluid accelerates as homogeneously stiff mass. Equation (2.18) can then be integrated along the flow path from an arbitrary starting point $x = l_1$ to $x = l_2$, obtaining

$$M(l_1, l_2) \frac{dq}{dt} = p(l_1) - p(l_2) - F(q, \mu, l_1, l_2) + G(l_1, l_2, \rho) \tag{2.19}$$

where

$$M(l_1, l_2) = \int_{l_1}^{l_2} \frac{\rho(x)}{A(x)} dx$$
$$F(l_1, l_2, q, \mu) = \int_{l_1}^{l_2} \frac{\partial \tau}{\partial x} dx$$
$$G(l_1, l_2, \rho) = \int_{l_1}^{l_2} \rho(x) g \cos(\phi(x)) dx.$$

The parameter $M(l_1, l_2)$ is the integrated density per cross-sectional along the flow path, $F(l_1, l_2, q, \mu)$ is the integrated friction along the flow path, and $G(l_1, l_2, \rho)$ is the total gravitational effects on the fluid.

2.3.1 Drill string and annulus

The flow through the drill bit can be modeled using equation (2.19) resulting in

$$M(h_r)\dot{q}_{bit} = p_p - p_0 - F(h_r, q_{bit}, \mu) + G(h_r, \rho, l_{bit}) \tag{2.20}$$

where p_0 is the atmospheric pressure from the fact that the annulus is open to the atmosphere, $F(h_r, q_{bit}, \mu)$ is the total frictional pressure loss in the drill string and annulus, and $G(h_r, \rho)$ is the difference in hydrostatic pressure between the drill string and annulus at depth l_{bit}, and $M(h_r)$ is given as

$$M(h_r) = \int_0^{l_{bit}} \frac{\rho_d(l)}{A_d(l)} dl + \int_{h_r}^{l_{bit}} \frac{\rho_a(l)}{A_a(l)} dl.$$

In addition to the differential flow equation, the pressure at any location in the well is given by a steady state momentum balance. In the annulus it is on the form

$$p_a(l) = p_0 + F_a(l, h_r, q) + G_a(l, h_r)$$

where $F_a(l, h_r, q)$ is the frictional pressure drop, and $G_a(l, h_r)$ is the hydrostatic pressure, from the top of the annulus to the depth l. An similar relationship exists for the pressure in the drill string is given as

$$p_d(l) = p_p - F_a(l, h_r, q) + G_d(l, h_r)$$

where $F_d(l, h_r, q)$ is the frictional pressure drop, and $G_d(l, h_r)$ is the hydrostatic pressure, from the topside mud pump to the depth l.

2.3.2 Return line

Similarly, as for the flow trough the drill bit, the flow through the subsea pump and return line can be described as

$$M_{ssp}(h_r)\dot{q}_{ssp} = p_r(h_r, h_{ssp,in}) + \Delta P(\omega_{ssp}, q_{ssp}) - F_r(h_r, q_{ssp}, \mu) - G(h_{ssp,out}, \rho) \tag{2.21}$$

where $\bullet_{ssp}$ denotes the subsea pump, $p_r(h_r)$ is the riser pressure at the pump inlet $h_{ssp,in}$, ΔP is the differential pressure over the pump, $F(h_r, q_{ssp}, \mu)$ is the frictional pressure loss in the return line and $G(h_{ssp,out}, \rho)$ is the hydrostatic pressure at the pump outlet $h_{ssp,out}$. The pressure $p_r(h_r)$ is simply given as the hydrostatic pressure at the pump inlet

$$p_r(h_r) = \rho g(h_{ssp,in} - h_r)$$

and the parameter $M_{ssp}(h_r)$ is given as

$$M_{ssp}(h_r) = \int_{h_r}^{h_{ssp,in}} \frac{\rho_r(l)}{A_r(l)} dl + \int_0^{h_{ssp,out}} \frac{\rho_{rl}(l)}{A_{rl}(l)} dl$$

where rl denotes *return line*.

Similarly, the flow dynamics in the booster line is described as

$$M_b(h_r)\dot{q}_{bo} = p_{bp} - p_0 - F(h_r, q_{bp}, \mu) + G(h_r, \rho, l_{bo})$$

where p_{bo} is the pressure at the booster pump outlet.

2.3.3 Hydrostatic pressure

It is assumed that the riser is vertically mounted, such that the $\cos(\phi(x))$ term in the simplified flow dynamics is equal to 1.
For the drill string the hydrostatic pressure at location l is given as

$$G_d(l) = \rho g h(l).$$

The hydrostatic pressure in the riser at location l is given as a function of the riser height h_r on the form

$$G_a(h_r, l) = \rho g(h(l) - h_r). \tag{2.22}$$

The total hydrostatic pressure difference in 2.19 is then given as

$$G(l, h_r) = G_d(l) - G_a(h_r, l)$$

Similar expressions are found for the hydrostatic pressure in the booster line and return line.

2.3.4 Friction

The terms $F(q, h_r, \mu)$ in the flow dynamics denotes the pressure drop due to friction which is directly related to pressure drop, also known as head loss during flow through pipes and ducts. As stated, an accurate friction model, can account for the simplifications done in the model development. A number of models describing friction in general pipe systems systems exist in the literature, e.g in White (2011) and the model accuracy usually comes at the cost of complexity. In general drilling fluids are non-Newtonian and the flow contains

both laminar and turbulent flow segments and transitions between them. This makes high accuracy modeling of frictional losses a challenge. According to Stamnes et al. (2012) a modified version of the Herschel-Bulkley model is the industry choice for high accuracy. In the same paper, Stamnes suggest a model for Newtonian drilling fluids.

To determine if the flow regime is laminar or turbulent, the Reynolds number is calculated

$$Re(l) = \frac{4\rho q}{\pi d(l)\mu}$$

where $d(l)$ is the pipe inner diameter, and $\mu(l)$ is the viscosity, at location l. If the Reynolds number is below the critical value $Re_{crit} = 2300$ the flow is deemed laminar, and if above, turbulent. The pressure loss is obtained using the Darcy- Weisbach equation

$$F(l,q) = \int_0^l f(l)\frac{8\rho q^2}{\pi^2 d(l)^5} dl \tag{2.23}$$

with the friction factor $f(l)$ given as

$$f_{\text{laminar}}(l) = \frac{64}{Re(l)}$$

for laminar flow and

$$f_{\text{turbulent}}(l) = \left(-1.8\log\left[\frac{6.9}{Re(l)} + \left(\frac{\epsilon}{3.7d(l)}\right)^{1.11}\right]\right)^{-2}$$

for turbulent flow, where ϵ is the pipe wall roughness.

This is a fairly complicated model, relying on in-depth system knowledge. Parameters such as pipe wall roughness and viscosity are not necessarily known, and typically prone to change over time. Therefore, friction models are usually determined based on experimental results and empirical relations. In Çengel and Cimbala (2010) it is stated that an error of 10 % or more in friction factors using friction relation such as the one above is the norm rather than the exception.

Simplified Friction Model

A simpler steady state friction model can be found by approximation the frictional pressure loss as a function of flow rate only. Stamnes (2011) simplifies the pressure drop in the drill string and annulus to be quadratic in the flow rate. This model is based on dividing pressure loss into major and minor losses. Minor losses are related to losses due to bends and flow obstructions, while major losses are related to losses in straight sections. The author proposes the following simple friction model

$$F(q) = F_1 q^2 \tag{2.24}$$

However, Stamnes states that the parameter F_1 changes with operational conditions, and must be adapted or fitted using experimental data.

2.4 Subsea Pump

The subsea pump used for the mud return system is a dynamic pump. As opposed to positive displacement pumps (PDPs) where the fluid is directed into a closed volume and forced along by volume changes, dynamic pumps add momentum to the fluid by means of fast moving blades. Dynamic pumps generally provide a higher flow rate than PDPs, with a much steadier discharge. The dynamics pump type used in the DGD system for this case is a centrifugal pump. As seen in figure (2.2) fluid enters in the middle (the eye) of the pump, is flung around to the outside of the impeller blades, and discharged out the side of the pump.

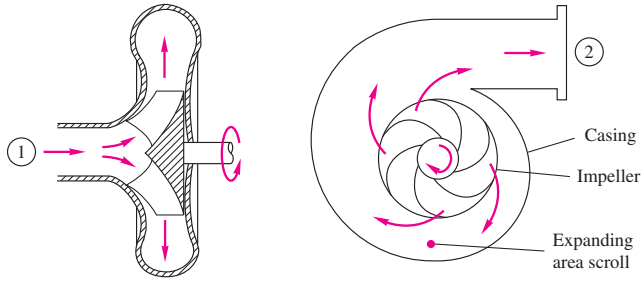

Figure 2.2: Side and frontal view of a typical centrifugal pump. Fluid enters axially in the middle of the pump, is flung around to the outside by the impeller, and is discharged out the side of the pump. Figure from White (2011).

The theoretical performance of a dynamic pump is given as a relationship between the produced head, h_{pump}, the flow rate through the pump, and pump rotational speed ω. The pump head is given simply as

$$h_{\text{pump}} = \frac{\Delta P_{\text{pump}}}{\rho g}$$

where ΔP_{pump} is the differential pressure over the pump. Curves describing this relationship can be plotted, and is known as the pumps performance curves or characteristic curves. An example is shown in figure (2.3). The maximum flow rate through the pump, called the pumps *free delivery*, occurs when there is no load on the pump. The other extreme, called the *shutoff head* occurs when the flow rate through the pump is zero, which is achieved when the pump inlet is blocked off. Between these two points, the pump head decreases with increasing flow rate.

A explicit expression for the pump head is of interest in order to identify the pump performance curves. The theoretical head as a function of flow rate and rotational speed can be

derived using the Euler turbomachine equations. A short derivation of the theoretical head for a centrifugal pump is given in appendix C, and the expression is given as

$$h_{\text{pump}} = \frac{r_2^2}{g}\omega^2 - \frac{\cot(\beta_2)}{2\pi b_2 g}\omega q. \tag{2.25}$$

where b_2 and r_2 is the blade width and impeller radius at the pump exit respectively. The theoretical pump head is seen to vary linear with the discharge flow rate, however this is usually not the case in reality. Additional losses due to e.g. friction affects the real pump head. To account for these effects an additional term, h_L, is added to equation (2.25) resulting in the following expression

$$h_{\text{pump}} = \frac{r_2^2}{g}\omega^2 - \frac{cot(\beta_2)}{2\pi b_2 g}\omega q - h_L(q). \tag{2.26}$$

The head is typically non-linear in terms of flow rate, as seen for the typical pump performance curve in figure (2.3), meaning h_L often includes a q^2 term. As for the case with friction models, this model is not particularly suited for system identification. It includes a lot of unknown parameters, which is not necessarily known beforehand, and is hard or impossible to isolate. A simpler model based on (2.26) is suggested in Stamnes et al. (2012). He presents a model for a typical centrifugal subsea pump used in DGD systems on the form

$$h_{\text{pump}}(\omega_{ssp}, q_{ssp}) = c_0\omega_{ssp}^2 - c_1\omega_{ssp}q_{ssp} - c_2 q_{ssp}^2 \tag{2.27}$$

where c_0, c_1, c_2 are lumped fitting constants which can be found using experimental data. The corresponding differential pressure over by the pump, which is the term included in the return line flow dynamics (2.21), is given as

$$\Delta P(\omega_{ssp}, q_{ssp}) = \rho g(c_0\omega_{ssp}^2 - c_1\omega_{ssp}q_{ssp} - c_2 q_{ssp}^2)$$

2.4.1 Operational point

The pumps operating point is determined by matching the system head (required head), h_{sys}, to the pump head (available head). The system and pump head intersects at one point determined by friction losses and elevation changes as seen in the example pump characteristics in figure (2.3). For the DGD mud discharge system, the system head is given as

$$h_{\text{sys}}(q_{ssp}) = \frac{1}{g\rho_{ssp}}\left[G_{rl}(h_{ssp}) + F_{\text{dis}}(q_{ssp}) - (G_r(h_{ssp}, h_r) - F_{\text{suc}}(q_{ssp}))\right] \tag{2.28}$$

where G_{rl} is the hydrostatic pressure just downstream the pump defined as $G_{rl} = \rho g h_{ssp,out}$ and G_r is the the hydrostatic pressure in the riser at the inlet defined in (2.22). F_{dis} and F_{suc} is the friction in the discharge and suction line respectively. By merging the suction line and return line the expression reduces to

$$h_{\text{sys}}(q_{ssp}) = \frac{1}{\rho g}[G_{\text{outlet}} - G_{\text{inlet}}(h_r) + F(q_{ssp})].$$

which is the friction and hydrostatic pressure terms included in the return line flow dynamics (2.21).

For steady state conditions a pump can only operate along its performance curves. The operational point of the pump is given as the flow rate at the intersection, q^*_{ssp} as seen in figure (2.3). The transients in flow dynamics is captured by the return line flow equation (2.21). If the system curves is not strictly decreasing the situation where the system curve intersects the pump curve at mote than one operating point. In this case the system may jump between the two points leading to a unstable system. Consequently, the model coefficients in equation (2.27) is required to be positive or zero

$$\{c \in \mathbb{R}^3 : c > 0\}, \; c = [c_0 \; c_1 \; c_2]^\top$$

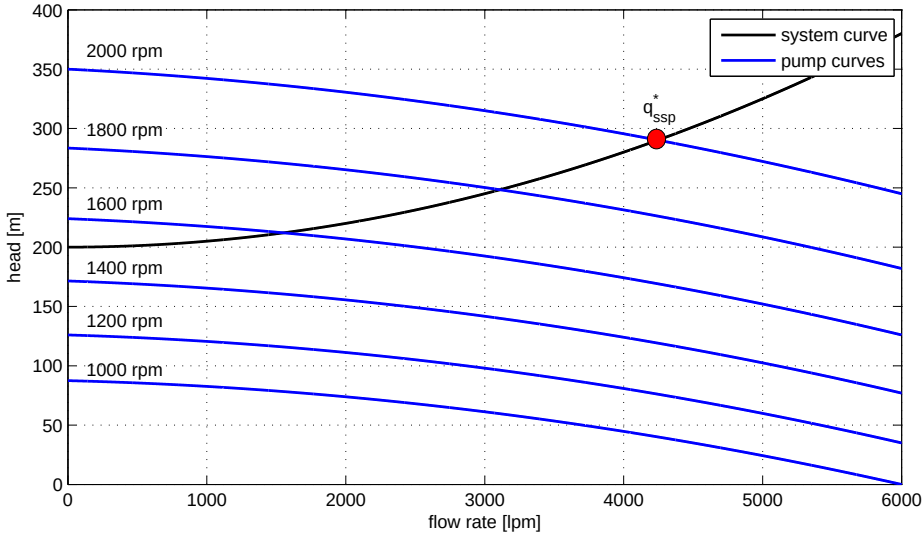

Figure 2.3: Synthesised example of pump characteristics for different speeds. Where the pump and system head intersects, marked with a red circle, is the pumps steady-state operational point.

2.4.2 Control System

The pump is typically controlled by a frequency converter which maintains a certain pump speed, ω_{ssp}. In Stamnes et al. (2012) is assumed that the pump converges to the reference speed, ω^{ref}_{ssp}, after a transient period τ_{ssp} and that the dynamics can be modeled as a first order system on the form

$$\tau_{ssp}\dot{\omega}_{ssp} = -\omega_{ssp} + \omega^{ref}_{ssp}, \qquad \frac{\omega_{ssp}}{\omega^{ref}_{ssp}}(s) = \frac{1}{\tau_{ssp}s + 1} \tag{2.29}$$

where the pump flow rate is found by solving the implicit equation

$$h_{\text{sys}}(q^*_{ssp}) = h_{\text{pump}}(\omega, q^*_{ssp}). \tag{2.30}$$

If the flow dynamics (2.21) is fast, an alternative to the flow dynamics is to solve (2.30), for the given pump speed, and if needed, add the simple first order dynamics (2.29).

The subsea pump is typically controlled using a standard PI controller. The controlled variable (CV) can i.e. be the riser pressure, and the pump reference speed is given as

$$\omega^{ref}_{ssp} = K_p \left(e(t) + \frac{1}{T_i} \int_0^t e(\tau) d\tau \right) \tag{2.31}$$

with the error defined as the deviation in riser pressure $e(t) = p_r(t) - p_r^{ref}$.

2.5 U- tubing

When two fluid columns are connected at the bottom, the level in the columns will equalize until the hydrostatic pressure at the bottom of each column is the same. This phenomenon is often referred to as U-tubing because the shape of the two connected fluid columns resembles a "U-Tube".

This effect is a common issue in drilling, especially in DGD where the fluid level in the riser is lowered. When the rig-pump is running on low speed or is shut off, the annulus and drill sting is connected through the drill bit at the bottom of the well. The bottom well pressure in the annulus will be different from the the bottom pressure in the drill sting due to the difference in column heights. This pressure difference triggers a flow from the drill string into the annulus until the pressure is equalized. The same is the case for the booster line when the booster pump is shut off. A potential problem with U-tubing is the fact that it might mask a kick. A common kick indicator is to check if the well is flowing when the pumps are shut of. With U-tubing present one can not immediately tell if the flow is caused by a kick, U-tubing or both.

Anfinsen (2012), presents a model used to estimate the effects of U-tubing in the drill string for a DGD system, and the main points are summarized here. The general model for the pressure and flow dynamics, valid for normal operations when the rig pump is running normally, is practically the same as the one derived in previous sections. However, he uses a hybrid system formulation, dividing the model into two operating conditions; pressure and level dynamics. Depending on the mud pump pressure p_p, the dynamics change. For the pressure dynamics where the rig-pump is operating under normal condition, U-tubing is not present, and the standard model is used with the level in the drill string are set to $\dot{x}_d = 0,\ x_d(0) =$ and $\dot{x}_b = 0,\ x_b(0) = 0$. When the rig pump ramps down, while still being sealed from the atmosphere, the drill string pressure will start to drop due to mud exiting. The level dynamics are entered when drill string top pressure reaches the the mud vapor pressure p_{vp}. When this happens, the level in the drill string starts to drop, and U-tubing is present. During U-tubing the drill string top pressure are kept at the vapor pressure as mud is evaporated to maintain the pressure. The level dynamics mode is given as

$$
\begin{aligned}
\dot{q}_{bit} &= \frac{1}{M(h_r)}\left(p_d - p_0 - F(q) - gh_{bit}(\rho_d - \rho_a) - \rho_d g h_d + \rho_r g h_r\right) \\
\dot{h}_d &= \frac{1}{A_d}(q_{bit} - q_p) \\
\dot{h}_r &= \frac{1}{A_r}(q_{ssp} - q_{bit} - q_{boost} - q_{tf}) \\
\dot{p}_d &= Kz(p_0 - p_d)
\end{aligned}
$$

where p_d is initialized as the mud vapor pressure p_{vp}, when the system enters the level dynamic mode, and z is a boolean value changing from 0 to 1 when the rig-pump is disconnected and the drill string is open to the atmosphere. K_1 is chosen sufficiently large to approximate instantaneousness change in p_p for disconnections.

U-tubing is discussed more in the next chapter where, the U-tubing effect is present in the booster line. The model presented here is however easily modified to describe the booster line.

2.6 Model Reduction and Summary

In this chapter a complete fit for purpose model has been derived for the DGD system. Further in this thesis the focus is on system identification. Real measurement data is used to estimate unknown parameters. The data is however only related to the mud-circulation part of the system. That, is dynamics related to the riser, and return line. Consequently, the flow and pressure dynamics in the drill string and annulus is not considered further. The states in the reduced system is the fluid level in the riser, h_r, and return line flow, q_{ssp}.

$$\dot{h}_r = \frac{1}{A_r}\left(q_{ssp} - q_{boost} - q_{tf}\right) \tag{2.32}$$

$$\dot{q}_{ssp} = \frac{1}{M_{ssp}(h_r)}\left(p_r(h_r) + \Delta P_{ssp}(q_{ssp}, \omega_{ssp}) - F(q_{ssp}) - \rho g h_{ssp,out}\right) \tag{2.33}$$

with

$$\Delta P_{ssp}(q_{ssp}, \omega_{ssp}) = \rho g(c_0\omega_{ssp}^2 - c_1\omega_{ssp}q_{ssp} - c_2 q_{ssp}^2)$$

Defining the state vector $\mathbf{x}^\top = \begin{bmatrix} h_r, & q_{ssp} \end{bmatrix}$, the non-linear model describing the mud circulation part of the system is given as

$$f(\mathbf{x}, t) = \begin{bmatrix} \frac{1}{A_a}\left(q_{ssp} - q_{boost} - q_{tf}\right) \\ \\ \frac{1}{M_{ssp}(h_r)}\left(p_r(h_r) + \Delta P_{ssp}(q_{ssp}, \omega_{ssp}) - F(q_{ssp}) - \rho g h_{ssp,out}\right) \end{bmatrix}$$

Chapter 3

System Identification

In this chapter, the unknown parameters of the mud circulation part of the system is identified, using the provided field data. This includes parameters both related to steady-state conditions and dynamics. Additionally, some parts of the model is revised. The system identification is performed using a "divide and conquer" approach. Different parts of the system is isolated using the measured data as input in order to estimate the parameters of the individual parts. All simulations are done in MATLAB and SIMULINK.

Remark. *The field data used in this section is sensitive and not open data. Because of this, all plots based on the data are masked. That is, the axis are given as a percentage. Plots with the same unit are scaled equally, such that comparison of the plots are possible. The identified parameters will not be listed either.*

3.1 Basic Theory

As a brief introduction to parameter estimation some central theory is included. More details can be found in i.e. Ljung (1999) and Ioannou and Sun (2012).

3.1.1 Least- Squares Estimation

Given a set of input and output (I/O) data obtained from a given system, the goal doing parameter estimation is, as stated in Ljung (1999), to find a model that produces small prediction errors when applied to the measurement data. The set of measurements is given as

$$\mathbb{Z}_N = \{y(1), u(1), y(2), u(2), \ldots, y(N), u(N)\}$$

where $y(\bullet)$ and $u(\bullet)$ is the system output and input respectively, at the sampling instants. Based on the measurement data the prediction error, given a certain prediction model $\hat{y}$, can be computed

$$\epsilon(t, \theta) = y(t) - \hat{y}(t).$$

And the sequence of prediction error can be written as a vector

$$V_N(\theta, \mathbb{Z}_N) = \frac{1}{N}\sum_{t=1}^{N} l(e(t,\theta)) \tag{3.1}$$

where $l(\bullet)$ is a scalar positive function. The basic idea behind the prediction error method is to find a the unknown parameters θ such that the prediction error become small in some sense. This is achieved by finding θ that minimizes (3.1)

$$\hat{\theta}_N(\mathbb{Z}_N) = \arg\min_{\theta} V_N(\theta, \mathbb{Z}_N).$$

This in in general a nonlinear optimization problem. However, when the proposed model structure is linear in the unknown parameters, the problem complexity is reduced. This is the case when the model is on the form

$$y(t) = \varphi^\top(t)\theta^* \tag{3.2}$$

where $\varphi(t)$ is called the regression vector and θ is the vector with unknown parameters. Using the predictor model

$$\hat{y}(t) = \varphi^\top(t)\theta \tag{3.3}$$

and by choosing $l(e) = \frac{e^2}{2}$, the prediction error (3.1) becomes

$$V_N(\theta, \mathbb{Z}_N) = \frac{1}{2N}\sum_{t=1}^{N}(y(t) - \varphi^\top\theta)^2.$$

This is a special case of the prediction error method called the Least- Squares (LS) method. Due to the linear model (3.3), the identification problem reduces to a linear regression problem. The LS estimate is denoted θ_N^{LS} and is given by

$$\theta_N^{LS}(\mathbb{Z}_N) = \arg\min_{\theta} \frac{1}{2N}\sum_{t=1}^{N}(y(t) - \varphi^\top(t)\theta)^2. \tag{3.4}$$

(3.4) is quadratic in θ and the global optimum optimal is found by by differentiating with respect to θ, resulting in the following expression for the optimal parameter estimate in the least square sense

$$\hat{\theta}_N^{LS} = \left(\frac{1}{N}\sum_{t=1}^{N}\varphi(t)\varphi^\top(t)\right)^{-1}\frac{1}{N}\sum_{t=1}^{N}\varphi(t)y(t) \tag{3.5}$$

For the solution (3.5) to exist, the the matrix $\frac{1}{N}\sum_{t=1}^{N}\varphi(t)\varphi^\top(t)$ must be invertible. To achieve this the regression vector $\varphi(t)$ must be sufficiently varied as a function of time, which is obtained if the input signal $u(t)$ is sufficiently rich.

3.1.2 Quality of Fit

The parameters estimated using equation (3.5) is optimal in a least- squares sense, but only for the given predictor model (3.3). If the model is poorly chosen, an optimal parameter estimate is indifferent. Depending on the model, the quality of fit varies. A measure on how good the estimator is compared to what is estimated is the mean squared error (MSE). MSE is a measure of the squares of the error and is a estimate of variance of residuals given as

$$MSE = \frac{1}{N}\sum_{t=1}^{N}(y(t) - \hat{y}(t))^2.$$

A high MSE value indicates that the model does not fit the observed data. Another related measure is the coefficient of determination, denoted R^2, which is a standardized measure indicating how well data fits a given model. This statistic indicates how closely values obtained from fitting a model, match the dependent variable the model it is intended to predict. The coefficient value ranges from 0 to 1, where 1 indicates a perfect model fit, and is given as

$$R^2 = 1 - \frac{SS_{res}}{SS_{tot}}$$

where

$$SS_{res} = \sum_{t=1}^{N}(y(t) - \hat{y}(t))^2$$
$$SS_{tot} = \sum_{t=1}^{N}(y(t) - \bar{y})^2$$

SS_{res} is the residual sum of squares while SS_{tot} is the total sum of squares, measuring the squared difference between each observed data point and the overall mean value of the observed data $\bar{y}$.

3.1.3 Recursive Parameter Estimation

In many applications, the system model might be known, but its parameters may be changing with time. Usually because of changing operation conditions, aging of equipment etc. To obtain estimates of a time varying parameter an estimation scheme that provides frequent estimates based on the system I/O data is needed. These parameter estimation methods are often referred to as on-line estimation schemes, and a variety of methods are described in Ioannou and Sun (2012). The one presented here is the recursive Least-squares method with forgetting factor, where the forgetting factor indicates how much older data is weighted when updating the estimate.

The same model form as in 3.2 is used, with a slight modification. Often the derivative

of the available I/O signals appear in the model. Direct differentiation of available signals should be avoided, and a way to do that is to filter both sides of 3.2 with a n-th order stable filter $\frac{1}{\Lambda(s)}$, where n corresponds to the order of differentiation. The filtered model is on the form

$$z(t) = \theta^* \phi^\top(t), \qquad z(t) = \frac{y(t)}{\Lambda(s)}, \qquad \phi(t) = \frac{\varphi(t)}{\Lambda(s)}$$

The continuous-time recursive LS method with forgetting factor is summarized in table (3.1). For the case of a forgetting factor $\beta = 0$, the algorithm reduces to the "pure" LS algorithm, which has the property of guaranteed parameter convergence (Ioannou and Sun (2012)).

Table 3.1: Continuous-time Recursive Least- Squares

Parametric model	$z = \theta^{*\top} \phi$
Estimation model	$\hat{z} = \theta^\top \phi$
Normalized estimation error	$\epsilon = \frac{z - \hat{z}}{m^2}$
Adaptive Rule	$\dot{\theta} = P \epsilon \phi$ $\dot{P} = \begin{cases} \beta P - P \frac{\phi \phi^\top}{m^2} P, & \text{if } \|\|P(t)\|\| \leq R_0 \\ 0 & \text{otherwise} \end{cases}$ where P is the covariance matrix.
Design Variables	$P_0 = P_0^\top > 0;\ m^2 = 1 + n_s^2$. n_s chosen so that $\frac{\phi}{m} \in \mathcal{L}_\infty$ $\beta > 0, R_0 > 0$

3.2 Sensitivity Analysis

Sensitivity analysis is a way of analyzing mathematical models to find which parameters are the most important and most likely to affect the model output the most. Based on a sensitivity analysis one can define the critical parameters to be estimated, and ignore or simplify less crucial parameters. Karnavas, WJ (2009) summarizes the the applications of a sensitivity analysis. Amongst the applications is to validate a mathematical models, detect strange or unrealistic behavior and suggest the accuracy to which the parameters must be calculated. If the sensitivity coefficients are calculated as a function of time, it can be seen when each parameter has the greatest effect. The parameter values should then be estimated from data at the time when they have most effect on the output.

The purpose of doing the sensitivity analysis prior to the system identification, is to get a indication of which parameters that must be estimated most accurately. And also to serve as a guideline for where most time should be devoted. A brief sensitivity analysis of the mud circulation system model is performed. The unknown parameters are the fitting constants related to the subsea pump model, $c_0,\ c_1\ c_2$, friction model parameters and the flow dynamics parameter $M_{ssp}(h_r)$. A few simplifications are done. The parameter M_{ssp} is considered constant and the friction model used in the analysis is the simplified model 2.24, which describes the pressure drop as quadratic in flow rate, multiplied by a parameter F. The analysis is done as presented in Khalil (2002). The original system is augmented by a sensitivity function $S(t)$, which provides a first order estimate of parameter variations on the solution of the original system. The augmented system is given as

$$\begin{aligned} \dot{x} &= f(t, x, \lambda_0), & x(t_0) &= x_0 \\ \dot{S} &= \left[\frac{\partial f(x,t,\lambda)}{\partial x}\right]_{\lambda=\lambda_0} S + \left[\frac{\partial f(x,t,\lambda)}{\partial \lambda}\right]_{\lambda=\lambda_0}, & S(t_0) &= 0 \end{aligned}$$

where λ are the system parameters and λ_0 is the nominal values for the parameters. For the system 2.32 and 2.33, $S(t)$ is given as

$$S = \begin{bmatrix} x_3 & x_5 & x_7 & x_8 & x_9 \\ x_4 & x_6 & x_8 & x_9 & x_{10} \end{bmatrix} = \begin{bmatrix} \frac{\partial h_r}{\partial M} & \frac{\partial h_r}{\partial c_0} & \frac{\partial h_r}{\partial c_1} & \frac{\partial h_r}{\partial c_2} & \frac{\partial h_r}{\partial F} \\ \frac{\partial q_{ssp}}{\partial M} & \frac{\partial q_{ssp}}{\partial c_0} & \frac{\partial q_{ssp}}{\partial c_1} & \frac{\partial q_{ssp}}{\partial c_2} & \frac{\partial q_{ssp}}{\partial F} \end{bmatrix}$$

The augmented system was simulated using nominal values for the parameters. The nominal parameter values used were found from a brief identification procedure. Consequently, the parameters are in the correct range of the true value, however they are not necessarily accurate. This is justified by the fact that the purpose of this analysis is to get a indication of the importance of the parameters, and to find to which degree of accuracy is needed during the following system identification. The system simulation are shown in figure (3.1). The figure depicts sensitivity of the riser level, to change in the parameters, for a step input in the pump speed of 10%. Multiple observations can be made. Firstly, the riser level is only sensitive to changes in M_{ssp} during transients. This is obvious as the parameter does not affect steady state conditions, as seen in equation (2.33). The other parameters affect steady state conditions. Secondly, parameters related to the system input, the pump speed, affects the solution significantly. Especially the c_0 parameter which

is proportional to the square of the pump speed has great effect. The parameters related to losses such as friction, c_2 and F, seems to have less effect, at least compared to the pump related parameters. The conclusion drawn from the brief sensitivity analysis, is that a accurate pump model is important and extra emphasis should be made in order to get a accurate model.

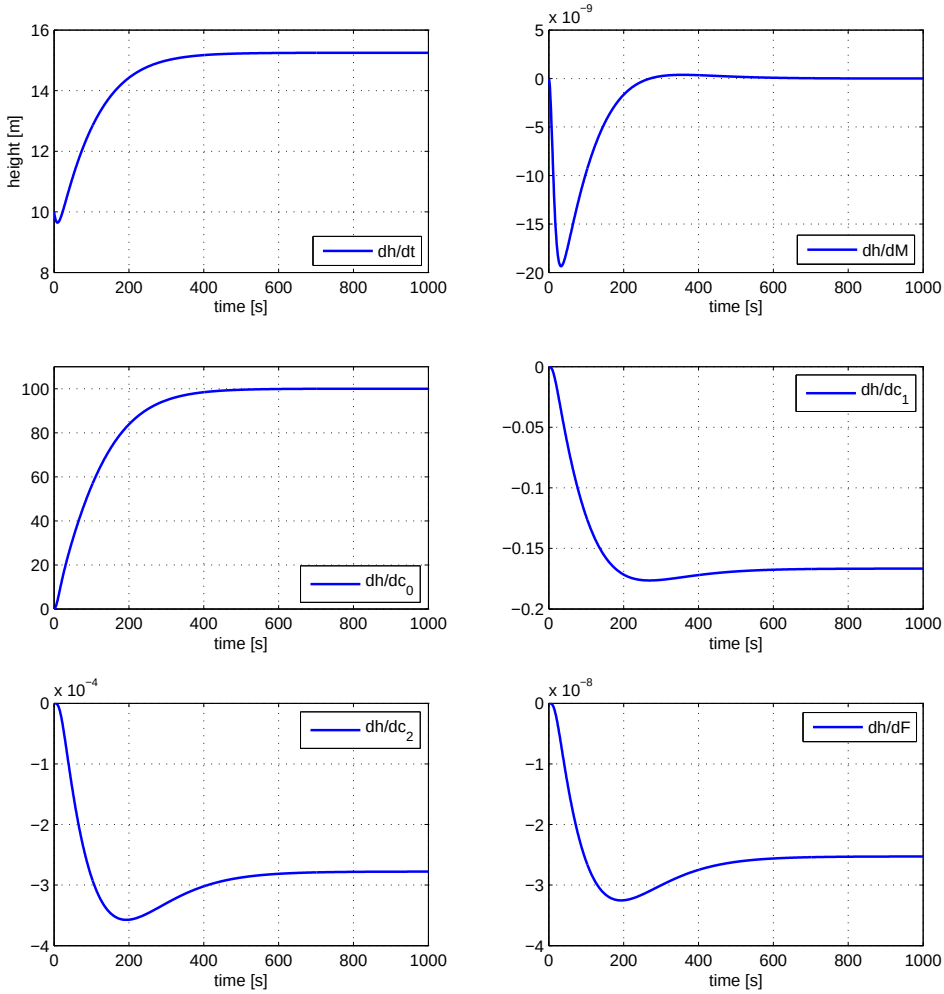

Figure 3.1: The upper left plot shows the riser level for a step change in pump speed. The other plots shows the sensitivities of the riser height with respect to the unknown parameters.

3.3 Setup and Measurements

The field data used for the validation and parameter identification of the DGD model is provided by Statoil ASA. They are logged during a non-drilling situation i.e. there is no drill string in the well and the BOP is sealed. A schematic of the setup is depicted in figure (3.2).

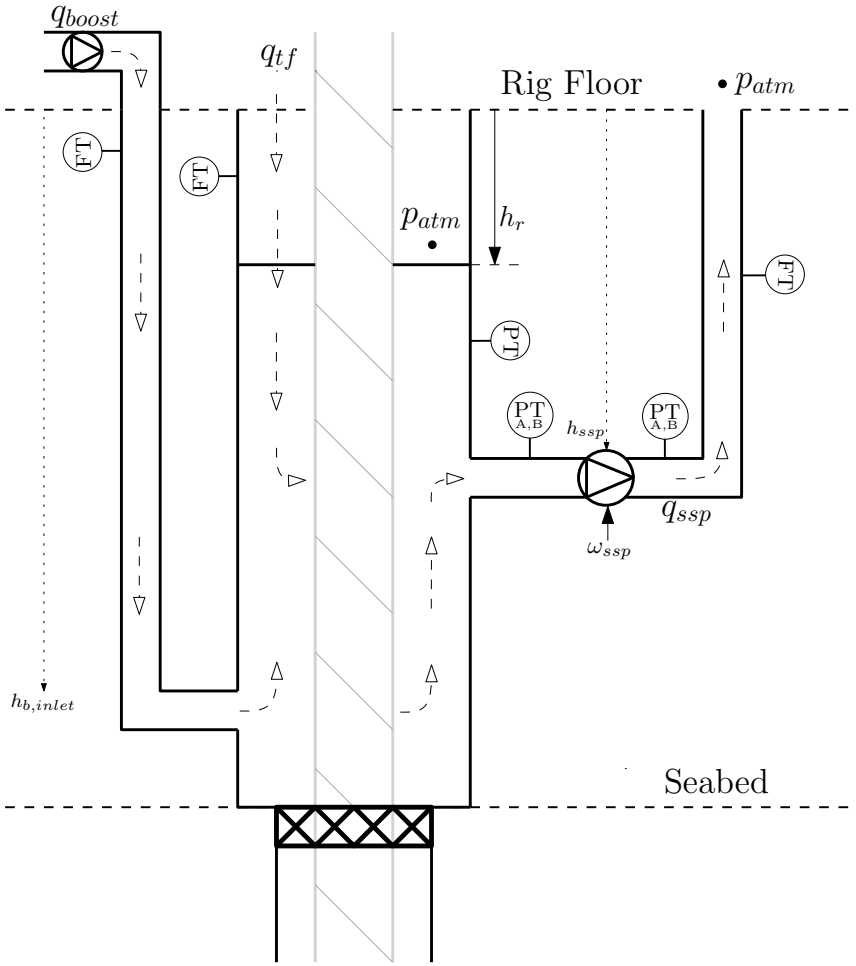

Figure 3.2: Schematic of the mud circulation system. Mud enters the riser from the booster line and top-fill and returns through the return line. Measurement points, and system states are indicated.

The mud is water-based with known density, $\rho = 1120\ \frac{\text{kg}}{\text{m}^3}$. It is circulated from the booster line which is a re-routed line from the mud-pump. However, the term *booster pump* will be used. During normal drilling operations flow from the booster line is used to help lift mud and cuttings up the riser, and is in this case the main input flow. The booster

line outlet enters the riser at at 340 mRKB, just above the wellhead at 352 mRKB. RKB, is short for *Rotary Kelly Bushing* and indicates the rig floor. Hence, mRKB is *meters below the rig floor*. In addition to the booster flow, the top-fill flow also enters the riser. The top-fill enters the riser from the top and is used to assure that the riser level does not drop too low unintentionally. The top-fill flow is usually kept at a constant low rate. The mud exits the riser through the return line, where the subsea pump is placed, with inlet 307 mRKB and outlet at 302 mRKB. The rotational speed of the subsea pump is controlled by a dedicated control system to maintain the desired riser pressure, which is the controlled variable (CV). The pump speed itself is not available, but the reference speed, ω_{ssp}^{ref}, from the control system is. The internal pump dynamics are considered very fast such that the true speed is considered to converge to the reference speed almost instantly. Hence, the internal dynamics are considered negligible and the reference speed is used as the true pump speed for identification purposes, denoted ω_{ssp}. The available measurements and the locations are summarized in table (3.2). Additional parameters regarding cross-sectional areas etc. can be found in appendix (A). The measurements are shown in figure (3.2), where FT denotes flow transmitter and PT denotes pressure transmitter.

Table 3.2: Available measurements

#	Name	Notation	Unit	Location
1	Riser pressure	P_r	[barA]	305 mRKB
2	Inlet pressure	P_{inlet}	[barG]	307 mRKB
3	Outlet pressure	P_{outlet}	[barG]	302 mRKB
4	Return flow	q_{ssp}	[lpm]	topside
5	Booster flow	q_{boost}	[lpm]	topside
6	Top-fill flow	q_{tf}	[lpm]	topside
7	Pump reference speed	ω_{ssp}^{ref}	[% of max]	-

When using measurements for system identification purposes, the estimated parameters are only as accurate as the measurements, and following is a short analysis of the different available measurements, pointing out the main errors.

3.3.1 Pressure measurements

The system has five dedicated pressure transmitters, one that measures the pressure in the riser at 305 mRKB, and redundant measurements at the subsea pump inlet and outlet. The riser pressure measurement are considered the most reliable of the five, as it measures the CV of the system. In order to check the consistency of the pressure measurements, they were compared with the riser measurement as reference for a stationary case. That is, when only hydrostatic pressure is present.

The redundant measurements at the inlet and outlet should ideally show the same value. However, due to what is assumed to be calibration error and possible other internal error

sources, this is not the case. In order to get a measure on the accuracy, the inlet measurements were compared to the riser pressure measurement, as shown in figure (3.4). The inlet pressures should measure a higher value as they are placed 2 meters deeper compared to the riser measurement, which corresponds to a difference in hydrostatic pressure of 0.22 bar. The top plot in figure (3.3) shows the pressure measurements for a period with no flow, and the lower plot shows the offset of the inlet measurements relative to the riser pressure measurement when the difference in height is corrected for. As seen, the inlet B measurement has a offset of 0.5 bar, while the inlet A measurement has zero offset. As a result the B measurement is disregarded and the inlet A measurement is the one used, as it is consistent with the riser measurement.

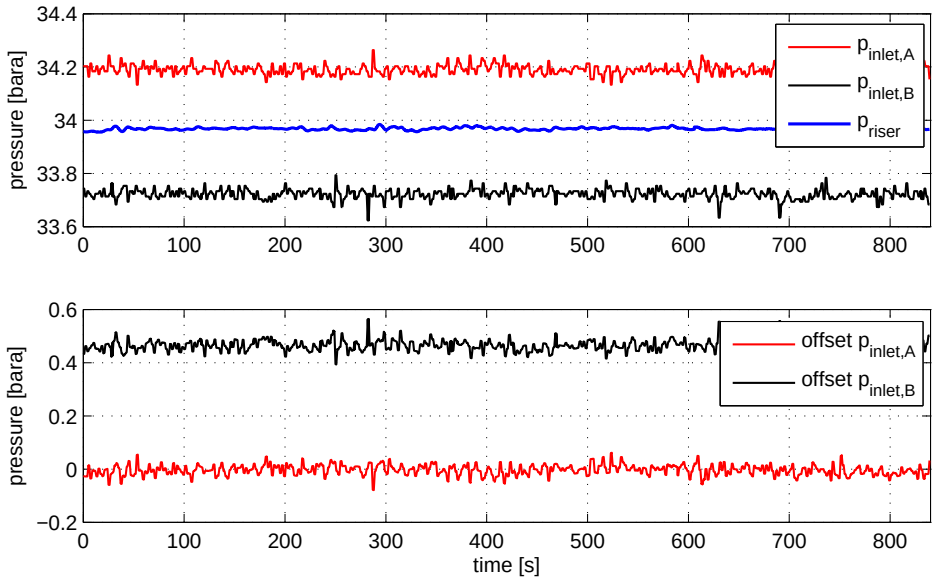

Figure 3.3: The first plot shows the inlet and riser measurements for a no-flow situation. In the second plot, the pump inlet pressure measurements are compared to the riser pressure measurement.

For the outlet pressure measurements a comparison to the hydrostatic pressure was done. Assuming that the return line is completely filled, the outlet pressure should correspond to the hydrostatic pressure for the same no-flow period as above. The A and B measurement differs somewhat, but the average of the two is consistent with the hydrostatic pressure. Consequently, the average is used.

3.3.2 Flow measurements

There are flow data available for the booster pump flow, top-fill flow and return line flow. The top-fill and return flow are measured using a dedicated flow transmitter, whereas the booster pump flow is a calculated flow. The pump delivering the booster flow is a positive displacement pump where a given amount of mud enters a closed volume and pumped

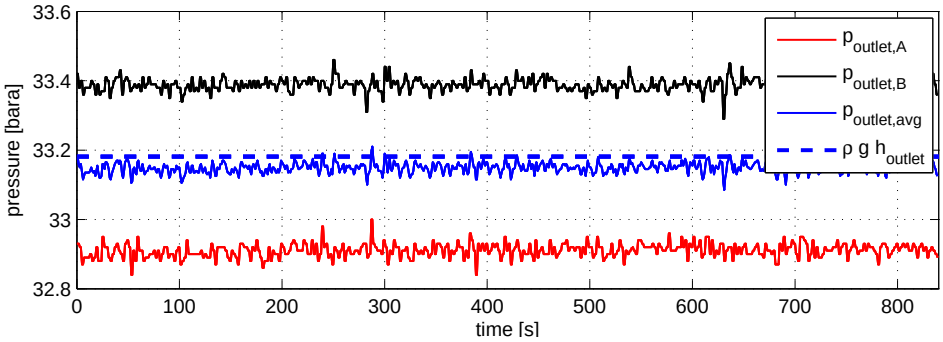

Figure 3.4: The pump outlet pressure measurements are compared to the hydrostatic pressure in the return line for a no-flow situation.

out by means of volume changes. The available booster pump flow rate is a calculated value based on the speed of the pump. Under normal conditions, where the pump have been operating with a given flow rate for some time, and the pressure at the pump outlet is high, the calculated flow rate is considered to be very accurate. However, a known source of error is when the pressure at the pump outlet is low, the volume of the pump chamber might not be completely filled. Consequently, the calculated flow will be inaccurate. Low outlet pressures can typically occur during U-tubing, where the fluid level and pressure in the booster line drops, resulting in uncertainty related to flow rate values when ramping up the rig pump.

3.4 Friction Model

The pressure drop due to friction in the return line can be estimated using the the system head equation

$$h_{\text{sys}} = \frac{1}{\rho g}[G_{\text{outlet}} - G_{\text{inlet}}(h_r) + F(q_{ssp})].$$

The system head equation is a steady state equation, and for constant flow conditions in the return flow, h_{sys} is equal to the head generated by the subsea pump. That is, $\Delta P = \rho g h_{sys}$ is the differential pressure over the pump

$$\Delta P = G_{\text{outlet}} - G_{\text{inlet}}(h_r) + F(q_{ssp}).$$

The hydrostatic pressure at the pump outlet is constant, from the fact that the return line is open to the atmosphere, and the assumption that the return line is completely filled. The height of the pump outlet is also constant during normal operation. Hence, the outlet hydrostatic pressure is given as $G_{\text{outlet}} = \rho g h_{ssp,out}$. The hydrostatic pressure at the inlet is not constant, as it and will vary with the fluid level in the riser, and is given as

$$G_{\text{inlet}}(h_r) = \rho g(h_{ssp,in} - h_r).$$

where $h_{ssp,in}$ is constant. The differential pump pressure can then be described as

$$\Delta P = \underbrace{\rho g(h_{ssp,out} - h_{ssp,in} + h_r)}_{\Delta G} + F(q_{ssp}) \tag{3.6}$$

and the steady state pressure drop due to friction is then found as a function of the differential pump pressure and hydrostatic pressure

$$F(q_{ssp}) = \Delta P - \Delta G(h_r) \tag{3.7}$$

Using the available pressure measurements at the inlet and outlet, and the flow rate measurement in the return line, $F(q_{ssp})$ can be plotted as a function of flow rate. The result is shown in figure (3.6). The red dots corresponds to steady state flow conditions, meeting the constraint

$$\left| \frac{dq_{ssp}}{dt} \right| \leq \epsilon.$$

while the blue dots represents all flow rates. An example of extracted steady state flow rates are shown in figure (3.5).

The pressure drop looks to be quadratic in terms of flow rate as predicted in the simplified model (2.24). It is worth noting the fact that the frictional pressure drop during flow transients seems to have the same characteristics as for steady state. The fact that the data points for transients are spread with the same range as for steady state data in indicates that friction does not vary when accelerating the fluid. Other effects causing pressure loss, often present during transients, such as turbulent and viscous effects, are negligible.

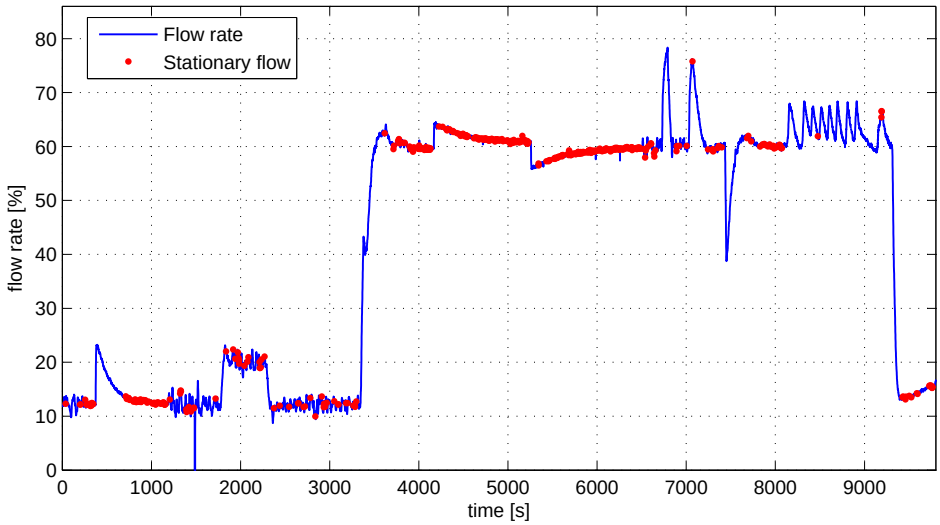

Figure 3.5: Example of extracted steady-state flow data.

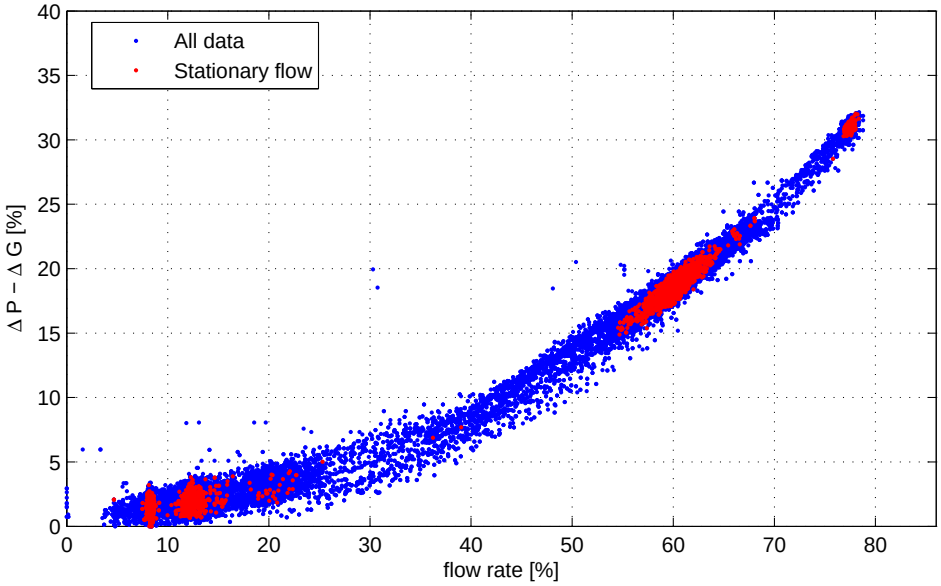

Figure 3.6: The frictional pressure drop in the return line as a function of flow rate. Red dots corresponds to steady-state flow, and blue is all available data.

Consequently, a steady state friction model should be sufficient.

In addition to the second order term in (2.24), a first order term is added to the model, and the data was fitted to a second order polynomial on the form

$$F(q_{ssp}) = F_1 q_{ssp} + F_2 q_{ssp}^2 \tag{3.8}$$

The friction coefficients F_1 and F_2 are found using LS method with the predictor model

$$\hat{y}(t) = \varphi^\top(t)\theta$$

with the measurements

$$y(t) = \Delta P - \Delta G(h_r), \qquad \varphi^\top(t) = \begin{bmatrix} q_{ssp} & q_{ssp}^2 \end{bmatrix}$$

and unknown parameter vector

$$\theta^* = \begin{bmatrix} F_1^* \\ F_2^* \end{bmatrix}$$

The estimation was done using both steady state and all data. The result from the estimation, that is the optimal parameters in a least-square sense θ^{LS}, is shown in figure (3.7). The resulting polynomial, using the estimated parameters F_1 and F_2 is shown in the top. As seen the estimated 2nd order model is accurate for most data, however not perfect. For high flow rates the estimate is below the measured pressure drop, and for flow rates in the range 30 - 50 %, the estimate is somewhat high. The model based on steady state data is practically identical to the one using all data, and the quality of fit coefficients is calculated to be

$$R^2 = 0.9929, \qquad MSE = 0.0504$$

which indicates a good model, but as pointed out from inspecting the plot, additional improvements can be done.

To improve the accuracy of the model, higher order polynomials is suggested. By experimenting with the order it was found that using a fourth order polynomial improved the estimate, and the accuracy gained when trying higher orders were negligible. The fourth order model corresponds to the following predictor model

$$\hat{y}(t) = \varphi^\top(t)\theta$$

with the measurements

$$y(t) = \Delta P - \Delta G(h_r), \qquad \varphi^\top(t) = \begin{bmatrix} q_{ssp} & q_{ssp}^2 \end{bmatrix}$$

and unknown parameter vector

$$\theta^* = \begin{bmatrix} F_1^* & F_2^* & F_3^* & F_4^* \end{bmatrix}^\top.$$

The augmented model is shown in the bottom plot of figure (3.7). From inspection it is obvious that the new model provides a better fit compared to the second order model. It

manages to reproduce the measured pressure drop for all measured flow rates.
By close inspection it can be observed that the estimated model bends slightly at low flow rates $< 10\ \%$, and that if not forced to start in zero, there would be a small offset. It is assumed that this is due to measurement error in the riser pressure. As the mud is water-based, stiction effects, sometimes observed in drilling systems at low flow rates, are assumed not present. The quality of fit coefficients confirms what is observed from the plot, as it is calculated to

$$R^2 = 0.9946, \qquad MSE = 0.0388$$

The estimated friction parameters are as mentioned not listed due to data sensitivity.

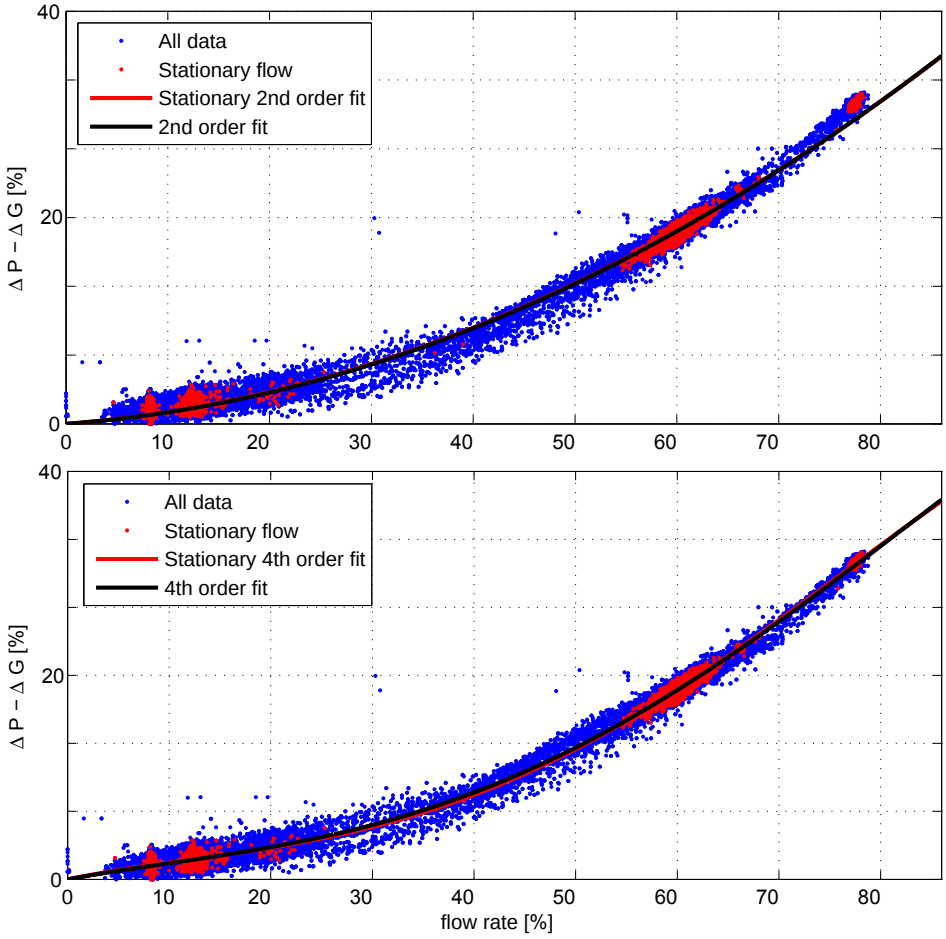

Figure 3.7: The upper plot shows a 2nd order model fitted to both steady-state, and all data. The lower plot shows the equivalent for a 4th order model.

3.5 Subsea Pump Model

In order to determine differential pressure over the subsea pump, for a given pump speed, the performance curves must be identified. The goal is to find a pump function describing the pump head as a function of pump speed and flow rate that is valid for all pump speeds. As stated in section (2.4) Stamnes et al. (2012) suggests the pump function

$$\Delta P_{ssp}(\omega_{ssp}, q_{ssp}) = \rho g(c_0\omega_{ssp}^2 - c_1\omega_{ssp}q_{ssp} - c_2 q_{ssp}^2)$$

which is based on a theoretical derivation of the pump head, with $c_0, c_1, c_2 \geq 0$. The constants c_0, c_1, c_2 are lumped parameters that must be estimated using experimental data. As with friction this can be done using standard LS estimation. The predictor model is defined with the measurements and unknown parameter vector

$$y(t) = \frac{\Delta P}{\rho g}, \quad \varphi^\top(t) = \begin{bmatrix}\omega_{ssp}^2, & -\omega_{ssp}q_{ssp}, & -q_{ssp}^2\end{bmatrix}, \quad \theta^* = \begin{bmatrix}c_0^* \\ c_1^* \\ c_2^*\end{bmatrix}.$$

When using all available measurement data and without restrictions on the sign of the fitting constants, the proposed best fit suggests a model where the c_1 parameter is negative. This results in the performance curves being is concave up. This is obviously an infeasible model, as the curves must be concave down. When including the constraint enforcing positive fitting constants, the cross term $\omega_{ssp}q_{ssp}$ is estimated to zero, that is $c_1 = 0$. Consequently, a reduced pump model is suggested on the form

$$\Delta P_{ssp}(\omega_{ssp}, q_{ssp}) = \rho g(c_0\omega_{ssp}^2 - c_2 q_{ssp}^2).$$

The predictor model was changed accordingly, and by using all available data the resulting pump curve function, $h_{\text{pump}}(\omega_{ssp}, q_{ssp})$ for a set of pump speeds, can be seen in figure (3.8).
The curves are plotted for different pump speeds, as indicated by a corresponding percentage at the zero-head line. The estimated pump curves are plotted with solid lines, and the actual measured head for the given flow rate and pump speed is plotted as dots. The colors indicates which speed the function and measurement data corresponds to. By inspection it is clear that the estimated function provides bad estimates for low pump speeds, and that the accuracy improves somewhat for higher speeds. Looking e.g. at the curve and data corresponding to 40% pump speed, the estimated head is significantly lower than the measured head. The quality of fit and MSE for the model is calculated to be

$$R^2 = 0.9602, \qquad \text{MSE} = 213.$$

As indicated in the sensitivity analysis, an accurate pump model is crucial to be able to accurately estimate the return line flow, q_{ssp}, and the above model is not deemed sufficiently accurate. By inspecting figure (3.8) it is observed that the shape of the curves fits the measured data, which indicates that the term $c_2 q_{ssp}$ is a good model term. The term $c_0\omega_{ssp}^2$, estimating the shutoff head, on the other hand need modification.

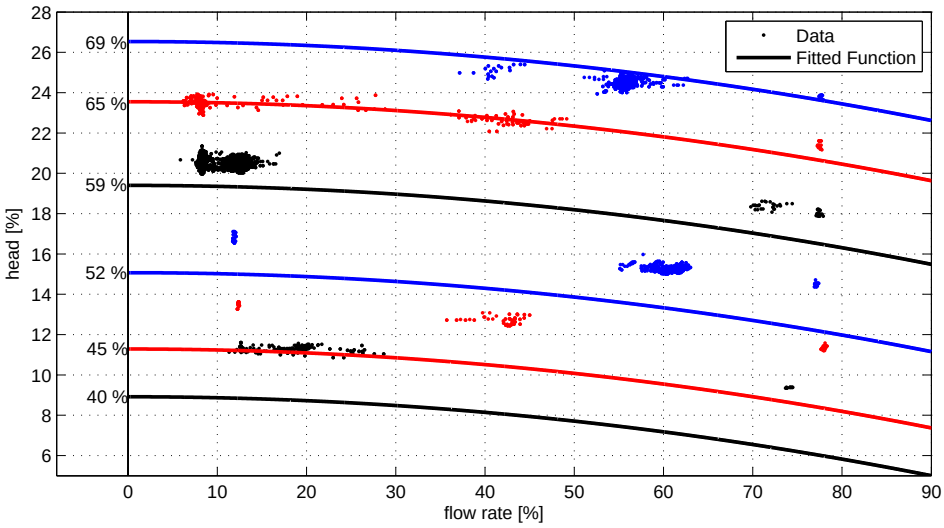

Figure 3.8: Subsea pump characteristics using the original model. The solid lines represents the estimated model for the different pump speeds indicated by the percentage at the zero-line. The dots represents measurement data for the same speeds.

3.5.1 Model Optimization

It is not to be expected that the performance curves found from measured data should match the theoretical model perfectly. Over time the pump will change characteristic because of wear and tear, and a more flexible model is needed. By investigating different approaches for model altering, it was found that by changing the exponent of the pump speed could improve the model. A revised model with an additional degree of freedom is suggested on the form

$$\Delta P_{ssp}(\omega_{ssp}, q_{ssp}) = \rho g(c_0 \omega_{ssp}^k - c_2 q_{ssp}^2).$$

In order to determine the best value for the exponent k, an optimization problem is formulated where the cost function is the MSE value from the LS estimation for a given model. The optimization problem is given as

$$\begin{aligned} &\min_{k,c_0,c_2} \frac{1}{N} \sum_{t=1}^{N} (\Delta P - \Delta P_{ssp}(\omega_{ssp}, q_{ssp}))^2 \\ &\text{s.t} \quad \{c \in \mathbb{R} : c > 0\},\ c = [c_0,\ c_2] \end{aligned}$$

with

$$y(t) = \frac{\Delta P}{\rho g}, \qquad \varphi^\top = \begin{bmatrix} \omega_{ssp}^k & -q_{ssp}^2 \end{bmatrix}, \qquad \theta^* = \begin{bmatrix} c_0^* \\ c_2^* \end{bmatrix}.$$

The optimization procedure itself was implemented using the *fminseach* function in MATLAB, which utilizes the *Nelder-Mead simplex direct search* algorithm. Similarly, as for the original model, the estimated pump curves from the new model are plotted for the set of pump speeds together with the measured head for the same speeds, and can be seen in figure (3.9). By inspection only, it is obvious that the revised model significantly improves the estimate. This observation is also confirmed looking at the quality of fit coefficients, which is calculated to

$$R^2 = 0.9991 \qquad \text{MSE} = 4.754,$$

where a significant reduction in model error is achieved.

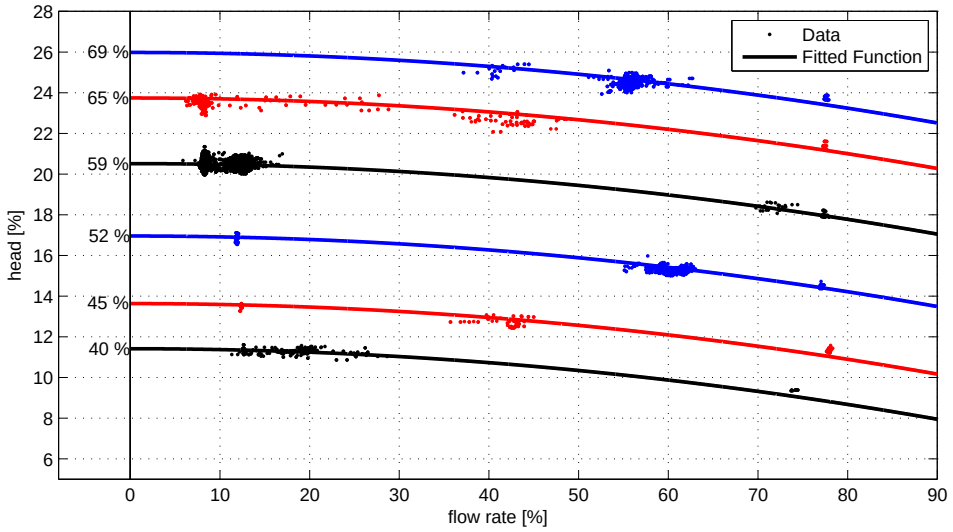

Figure 3.9: Subsea pump characteristics using the optimal model. The solid lines represents the estimated model for the different pump speeds indicated by the percentage at the zero-line. The dots represents measurement data for the same speeds.

Data Filtering

In addition to the model optimization, a data filtering procedure was done in order to investigate if the model could be further improved. The experimental data is not uniformly distributed in pump speed, head and flow rates. This causes the model to be most accurate for the parts where most data is available. Looking at figures (3.8) and (3.9), the measurement data appear in groups or clusters for a given head and flow rate. For some speeds, all available data corresponds to only one such cluster. When using data for those particular speeds the identification could yield poor result as any model can be fitted to a single point.

The filtering was done by finding speeds for which minimum three head- flow rate clusters was available e.g. as is the case for speeds 45% and 52% in figure (3.8) and (3.9). Post filtering, the same optimization procedure as above was done to find the optimal model. The result, plotted in figure (3.10), is similar to the one identified prior, with a slightly lower c_2 value, causing the performance curves to curve slightly less. The new model seems to correspond slightly better at higher flow rates, but as the cost of not being as accurate for lower flow rates. This is a result from the filtering, where speeds with data at high flow rates are more dominant compared to pre-filtering. However, when looking at the quality of fit measures the improvements by filtering data is not significant.

$$R^2 = 0.9988, \qquad \text{MSE} = 4.4118.$$

The R^2 value has actually decreased somewhat, while the MSE value is lower which is probably because of the reduction in amount of data used in the model identification.

The estimated parameters are as mentioned not listed due to data sensitivity.

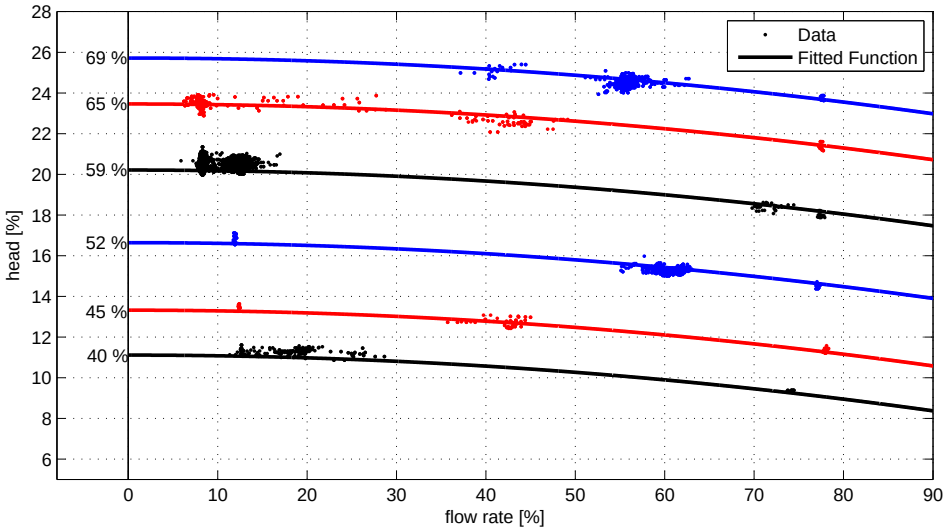

Figure 3.10: Subsea pump characteristics using the optimal model with filtered data. The solid lines represents the estimated model for the different pump speeds indicated by the percentage at the zero-line. The dots represents measurement data for the same speeds.

3.6 Level Dynamics

The level dynamics in the riser is described simply as the difference in flows in and out of the riser, proportional to the cross sectional area of the riser A_r

$$\dot{h}_r = \frac{1}{A_r}(q_{ssp} - \underbrace{q_{boost} - q_{tf}}_{q_{in}}).$$

The inner diameter of the riser is known and constant. Hence, so is the cross sectional area. Using the measured flow rates, the estimate of h_r should equal the level calculated form the riser pressure measurement, for normal a circulation case. That is, when the booster pump and top-fill flows are constant, and only the return line flow varies. With the initial conditions set to the measured level, $h_r(0) = h_{r,measured}(0)$ the riser level was simulated using the measured flows and compared to the measured level. The result is shown on figure (3.11).

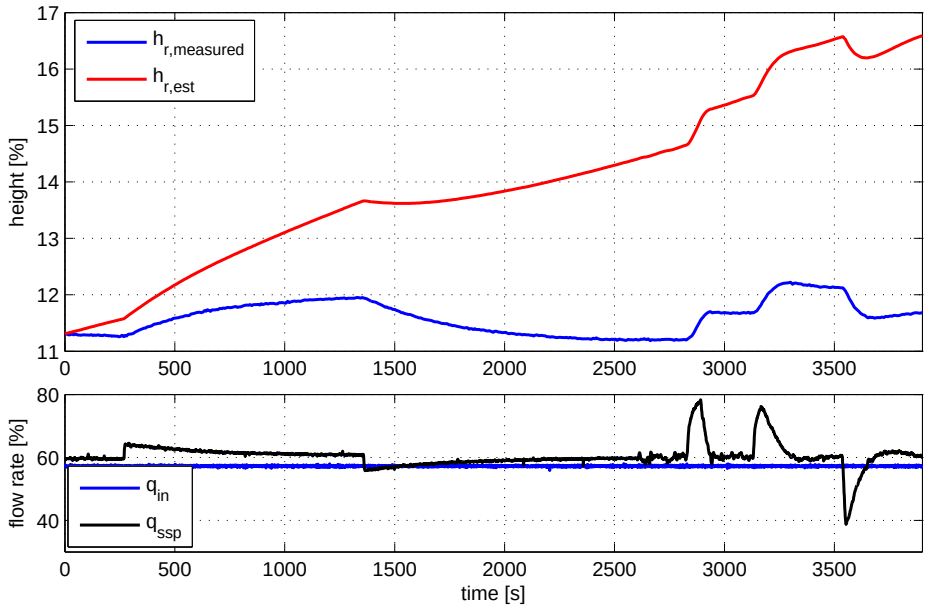

Figure 3.11: Isolated level dynamics for a normal circulation case. The upper plot shows the measured and estimated riser level. The lower plot shows the input-flow and return flow used.

The level estimate diverges as there is no sort of feedback stabilizing the isolated model, indicating that measured in-flow does not equal measured out-flow. The divergence is not surprising, as the integration done to compute the level in the model is very sensitive to small errors. If $\dot{h}_r$ is not truly zero the estimate will diverge due to integration drift.
In a normal drilling situation, where cuttings and well influx are present, the in, and out flow is typically not equal, as the fluid density will differ. However when running the mud circulation system only there is no unknown influx, and the mud density is the same for

the whole system. Another cause of divergence is compressibility in a pressurized system where inlet and outlet pressures are different. As the flow is given in terms of volume flow, the volume flow in will differ from the volume flow out in this case. However, from the fact that the mud is water based and the annulus is open to the atmosphere, this is likely not the cause. Therefore, it is reason to believe that the flow measurements are biased or that there could be a leak causing a discrepancy between in and out flow measurements.

To account for the difference in flows, a correction factor θ is introduced

$$\dot{h}_r = \frac{1}{A_r}(\theta_1 q_{ssp} - q_{in}) \tag{3.9}$$

The correction factor could change for different conditions, and is not necessary constant. A recursive parameter estimator with forgetting factor was designed to identify the parameter and identify if the parameter fluctuates, and to what degree. The estimator was designed using the predictor model with the measurements and unknown parameter vector

$$\begin{aligned} \hat{y}(t) &= \varphi^\top(t)\theta \\ y(t) &= A_r\dot{h}_r + q_{in}, \qquad \varphi(t) = q_{ssp}, \qquad \theta^* = \theta_1^* \end{aligned}$$

and by using a simple first order filter, the model becomes

$$z(t) = \phi^\top(t)\theta^*, \qquad z = \frac{y(t)}{\Lambda(s)}, \qquad \phi = \frac{\varphi(t)}{\Lambda(s)}, \qquad \Lambda(s) = \frac{1}{5s+1}.$$

The recursive estimator was implemented according to the equations in section section (3.1.3), corresponding to normal circulation, using the following design parameters

$$m = 1, \qquad \theta_{1,init} = 1, \qquad P_0 = 10, \qquad \beta = 0.1.$$

The results for the given section of the data is shown in figure (3.12). The parameter estimate, shown in the bottom left plot, converges more or less to a constant value. Some fluctuations are observed, however to only a small degree. The result is consistent when using different data from similar normal circulation cases. The degree of fluctuation differs somewhat, but is centered around the same value. This is a clear indication that there is a constant bias in the flow measurements. The parameter is considered constant form here on, and set to

$$\theta_1 = 0.951$$

As seen the from the upper plot in the figure, the correction factor successfully accounts for the measurement error.

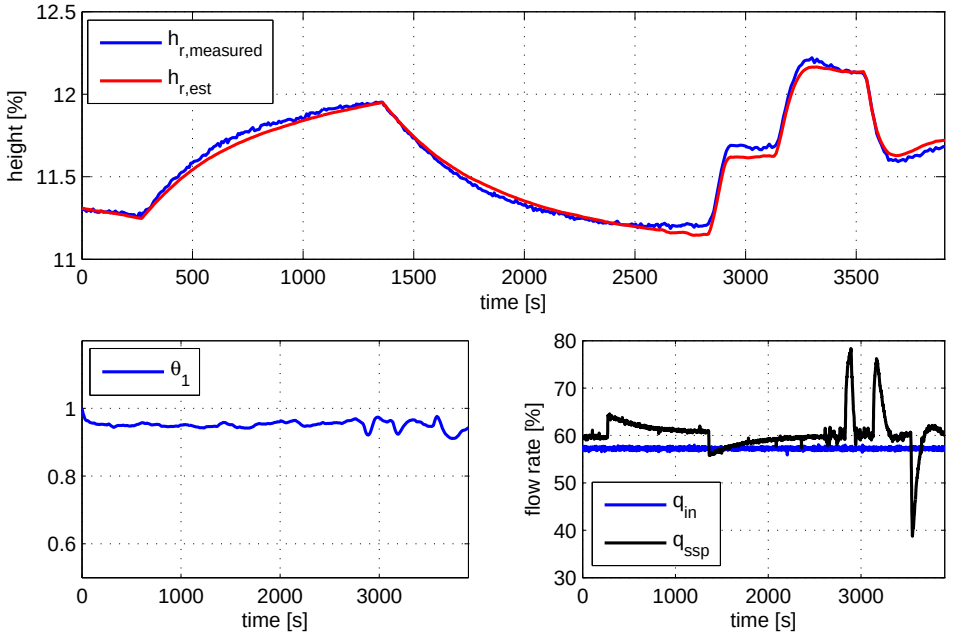

Figure 3.12: Isolated level dynamics for a normal circulation case with identified correction factor. The upper plot shows the measured and estimated riser level. The lower-left plot shows the estimated correction factor over time while the lower-right plot shows the input-flow and return flow used.

3.7 U-tubing

In the previous section the riser level was estimated for normal circulation, where the booster pump flow was maintained at a constant rate. For the case where the booster pump ramps down, the U-tubing effect is found to induce an additional unmeasured flow into the riser. In order to correctly estimate the riser level for this case the mentioned flow must be estimated. As the booster pump flow is not measured using a flow meter, but rather calculated from the pump speed, this extra flow is undetected. The flow has great effect on the fluid level in the riser, and the original model (3.9) is not valid without augmentation. The top plot in figure (3.14) shows the estimated and measured riser level for a case where the booster pump is ramped down. Recall that the fluid level is defined downwards from the top of the riser, and a higher level in the plots, is equivalent to a lower fluid column level. When the booster pump flow drops to zero, the estimated level instantly starts to increase, as the measured flow leaving the riser is significantly higher than the calculated flow entering. The real level on the other hand stays relatively constant, until the subsea pump starts ramping down. It is obvious that for this to be the case there must be a significant non-measured flow entering the riser. As for the previous section the measured return flow and top-fill flow is used in the simulations, in order to isolate the U-tubing effects.

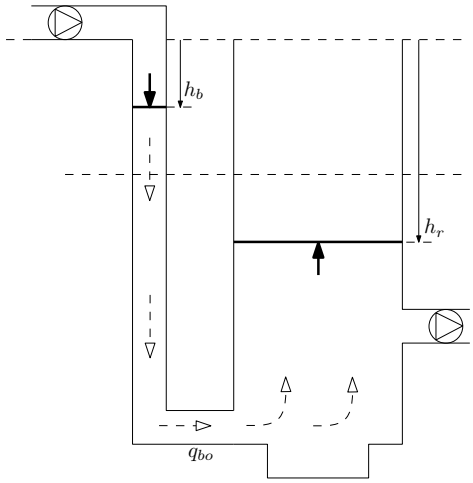

Figure 3.13: Schematic of the U-tubing effect in the booster line. The fluid level in the booster line drops and approaches equilibrium with the riser height, inducing a flow into the riser.

The flow due to the U-tubing effect can be estimated by calculating the flow needed to keep the measured riser level. The required flow, denoted q_U, can be found by including it in equation (3.9).

$$q_U = \theta q_{ssp} - q_{boost} - q_{tf} - A_r \dot{h}_{r,measured} \tag{3.10}$$

The estimated "missing flow", q_U, is shown in the bottom plot in figure (3.14). From the true flow rates in the data and the given cross-sectional area of the booster line, it is estimated that the required flow to keep the actual riser level causes the fluid level in the booster line drop drop roughly 160 m.

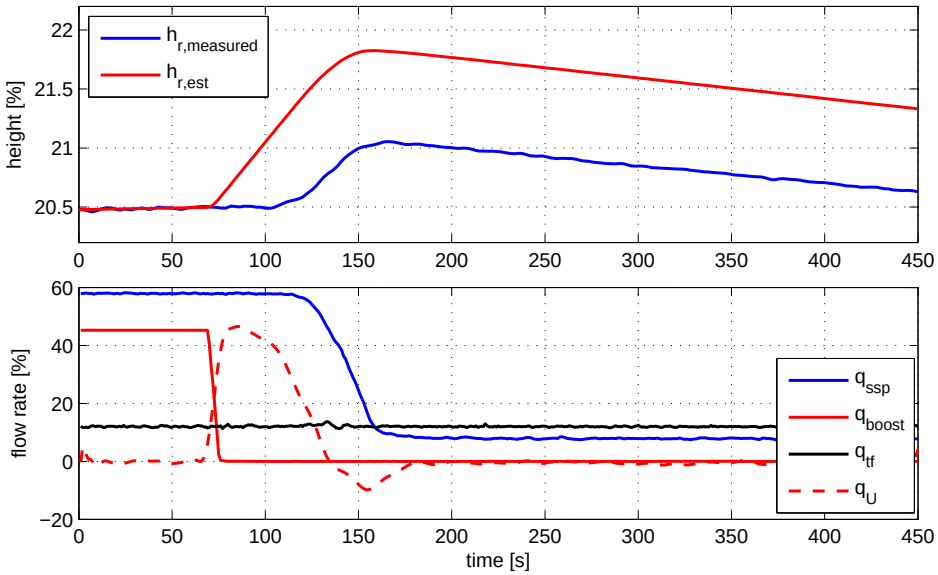

Figure 3.14: Example of the U-tubing effect, showing the "missing flow". The upper plot shows the measured and estimated riser level without accounting for the U-tubing effect. The lower plot shows the measured flows, and the extra flow, q_U, required to keep the measured riser level.

3.7.1 Booster Line Dynamics

When the booster pump is ramped down, it is assumed that the booster line is not completely sealed form the atmosphere. That is, the pressure at the top of the booster line turns atmospheric, and the fluid level in the booster line starts to drop, inducing a flow into the riser, as illustrated in figure (3.14). This is a simplification compared to the model in Anfinsen (2012). The pressure dynamics in the booster line is neglected as the pressure is assumed to instantly turn atmospheric when the booster pump is ramped down. Because of limited system information regarding the booster pump and, with no dedicated flow or pressure measurements, a more complicated model would be hard to validate. In order to estimate the flow due to the U-tubing effect two new states are introduced to the level dynamics. q_{bo}, defined as the flow entering the riser from the booster line, and the fluid level in the booster line, denoted h_b.

The flow dynamics is modeled according to the momentum balance (2.19). From the assumption of atmospheric pressure at the top of the booster line during U-tubing, the dynamics reduces to the difference in hydrostatic pressure in the booster line and riser, with an additional friction term.

$$\dot{q}_{bo} = \frac{1}{M_b(h_b)} \left(\rho g (h_r - h_b) - F(q_{bo}) \right). \tag{3.11}$$

As stated, this is a simplified version of the model presented in Anfinsen (2012), where it is assumed that the pump inlet is sealed from the atmosphere when U-tubing starts. The

pressure at the top of the booster line reaches vapor pressure, and mud starts to evaporate to maintain this pressure. These effects are neglected from the atmospheric pressure assumption.

The friction term $F(q_{bo})$ is assumed to be linear in terms of flow rate on the form $F(q_{bo}) = F_b q_{bo}$. Due to the lack of measurements, the parameter F_b reduces to a tuning parameter, as there is no way to estimate the pressure drop due to friction in the booster line. For the parameter M_b which relates to the flow dynamics, a estimate is found from the flow dynamics derivation

$$M_b(h_b) = \int_{h_b}^{l_{bo}} \frac{\rho(l)}{A_b(l)} dl$$

where l_{bo} is the depth of where the booster line enters the riser, which is at 340 m. Neither the cross sectional area or density of the mud is a function of depth and is given as the constants $A_b = 0.0103 \text{ m}^2$ and $\rho = 1120 \frac{\text{kg}}{\text{m}^3}$. A theoretical estimate of M_b is therefore given as

$$M_b(h_b) = \frac{\rho}{A_b}(l_{bo} - h_b).$$

The term depending on h_b is small compared to the constant term. Additionally, the dynamics are assumed to be very fast. Hence, $M_b(h_b)$ is considered constant in the model $M_b(h_b) = M_b$. The resulting height dynamics in the booster line and riser is given as

$$\begin{aligned} \dot{h}_r &= \frac{1}{A_r}\left(\theta_1 q_{ssp} - q_{tf} - q_{bo}\right) \\ \dot{h}_b &= \frac{1}{A_b}(q_{bo} - q_{boost}). \end{aligned}$$

The model was implemented both as a hybrid system, where the augmented level dynamics was used only when the booster pump flow was zero or the booster line was not completely filled. That is, when $q_{boost} = 0$ or $h_b > 0$. And also with the augmented level dynamics as a part of the original system without any switching. Both strategies yielded more or less the same results, and the model without switching was used further in this section.

Figure (3.15) shows the results using the augmented model for estimating the flow due to the U-tubing effect. The flow dynamic parameter M_b was set to $M_b = \frac{\rho}{A_b} = 4 \times 10^7$.The friction parameter F_{bo} was set by trial and error to be $F_{bo} = 6 \times 10^7$. As seen from the top plot in figure (3.15) the level estimate deviates from the measured value. When the booster pump ramps down, which is the same case as shown in figure (3.14), the estimate is not far off. In other words, the estimated U-tubing flow is not far off. However, when the pump ramps back up the estimated fluid level deviates greatly. This is a result of a low booster flow estimate. The fluid level in the booster line, shown in the bottom plot, shows that the level drop is significant, and that is approaches equilibrium with the riser level (levels on the plots use the same scale). It can also be observed that the booster line is filled very slowly when the booster pump is turned on, because of the underestimated booster flow.

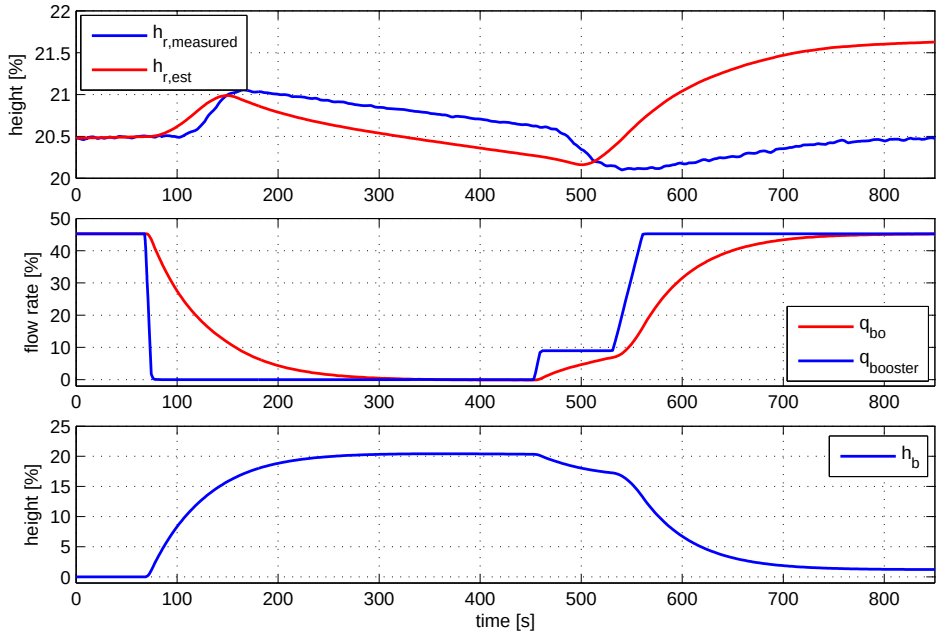

Figure 3.15: Simulation of the augmented riser level model. The upper plot shows the measured and estimated riser level. The middle plot shows the "measured" and estimated booster flow. The lower plot shows the estimated fluid level in the booster line.

Based on the previous model a new version is proposed. The main flaw with the original model was the low booster flow when the booster pump ramps up. This is solved by introducing a weighting parameter θ_b. Additionally, a weighting parameter is introduced to reduce the the booster line flow rate when the booster pump ramps down. The new model with the additional parameters is given as

$$\begin{aligned} \dot{q}_{bo} &= \frac{1}{M_b}\left(\rho g(h_r - \theta_{h_b} h_b) - F_b(q_{bo})\right) \\ \dot{h}_r &= \frac{1}{A_r}\left(\theta_1 q_{ssp} - q_{tf} - q_{bo}\right) \\ \dot{h}_b &= \frac{1}{A_b}(q_{bo} - \theta_b q_{boost}) \end{aligned} \tag{3.12}$$

The same case as above is used in the simulations. The results using the re-tuned model is shown on figure (3.16). Suitable values for the weighting parameters were found to be $\theta_{h_b} = 1.5$ and $\theta_b = 3.6$. As seen form the top plot, the riser height estimate is much improved both when ramping down and back up. An important observation is the fact that the estimated flow rate from the booster line is higher than the calculated booster pump flow value when the pump ramps up. This indicates that there are effects related to the booster-pump that is not accounted for in the model or that the booster pump flow values are not reliable when the pump ramps up. Looking at the un-tuned model simulations in figure (3.15) for comparison, the booster line flow is estimated significantly lower than the

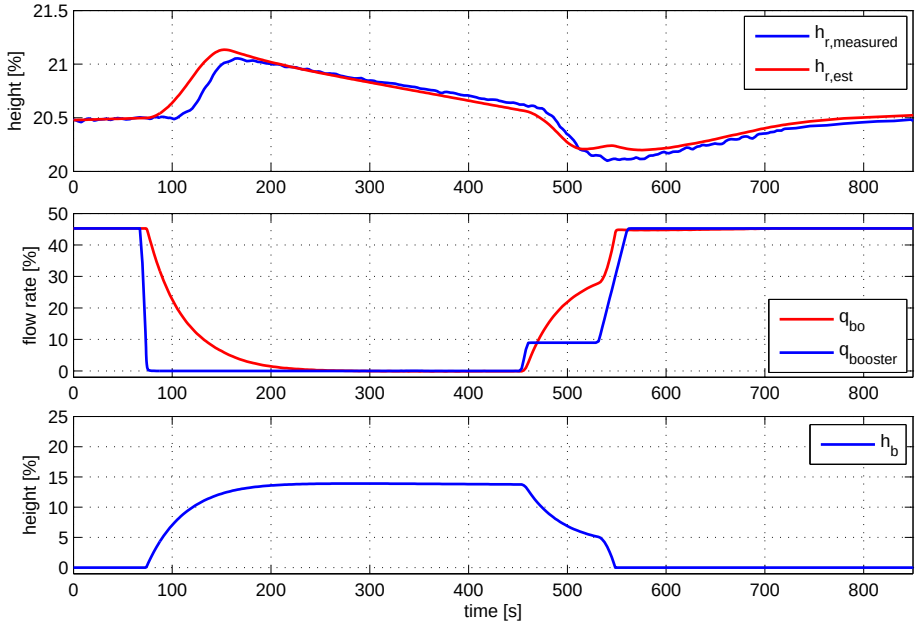

Figure 3.16: Simulation of the tuned augmented riser level model. The upper plot shows the measured and estimated riser level. The middle plot shows the ”measured” and estimated booster flow. The lower plot shows the estimated fluid level in the booster line.

calculated flow for the ramp-up part. Intuitively, this makes sense as there is a ”void” in the booster-line that must be filled up after U-tubing, before the the flow from the pump actually enters the riser and affects the level. However, as seen, a significantly larger flow is required. In other words, considerable uncertainty is related to U-tubing and the booster pump during ramp-up.

Another interesting point is that the estimated booster line level h_b is considerably lower compared to the un-tuned model. Thus, judging from the model, the riser and booster line level does not approach equilibrium. This could be an indication that the assumption of atmospheric pressure in the booster line is faulty, and that a more sophisticated model such as the one Anfinsen (2012) proposes possibly could capture more of unknown effects. However, with the lack of, and possibly faulty measurements related to the booster pump, the mentioned model is deemed too complicated. Instead and a simpler approach is pursued.

The tuned model (3.12) manages to estimate the flow from the U-tubing effect in addition to correct for uncertainty related to pump ramp-up. The drawback is the fact that it relies heavily on tuning of multiple parameters. Even though the weighting parameters were found to be consistent for all the cases of U-tubing found in the data, the model is overly complex. Also, by adding the tuning parameters the affiliation to the physical relations it was derived form fades. Because of this a more simpler approach was pursued

based on observations in the previous part. All U-tubing effect are lumped into simpler booster pump dynamics based on the the measured booster flow. The dynamics are divided into ramp-down and ramp-up cases.

3.7.2 Simplified Dynamics

Based on the simulations done with the above models a few observations are made, summed up in the following points:

1. When the booster pump ramps down the fluid level in the booster line drops and induces a flow from the booster line not present in the booster flow data. The simulations done with the above model shows that a significant flow is required in order to keep the riser level at the measured level.

2. When the pump ramps up, the booster line is filled. However, the booster flow needed to maintain the correct riser level exceeds the calculated booster pump flow. Consequently, it is assumed that the calculated flow leaving the booster pump is inaccurate in the transition until the flow reaches the pump flow set point, either because of calculation error, or unknown effects.

Ramping Down

Looking at figure (3.16), the estimated booster flow, q_{bo}, when the booster pump ramps down, resembles a first-order dynamic. The proposed model is on the form

$$\begin{aligned} \tau_b \dot{q_{bo}} &= -q_{bo} + q_{boost} \\ q_{bo}(s) &= \frac{1}{\tau_b s + 1} q_{boost}(s). \end{aligned}$$

where the time constant τ_b represents the time it takes for the booster line level, and booster flow to stabilize. The model was tested using a time constant of 40 seconds, an estimated value based on previous simulation i.e. as seen in figure (3.16). The result is shown in the upper left plot in figure (3.17). Not surprisingly, the estimated riser height resembles the ramp- down part from figure (3.17), and the estimate is considered decent. However, the estimated riser level still increases prior to the measured level. To correct this a time delay was added to the dynamics

$$q_{bo}(s) = \frac{e^{-\tau_d s}}{\tau_b s + 1} q_{boost}(s). \tag{3.13}$$

The 40 seconds time constant was split into the time delay $\tau_d = 30$ s and time constant $\tau_b = 10$ s. As seen in the upper right plot in figure (3.17), the added time delay improves the estimated level, removing the lag between the estimate and measured riser level. The values used for τ_d and τ_b is found to be consistent for all cases of U-tubing in the data.

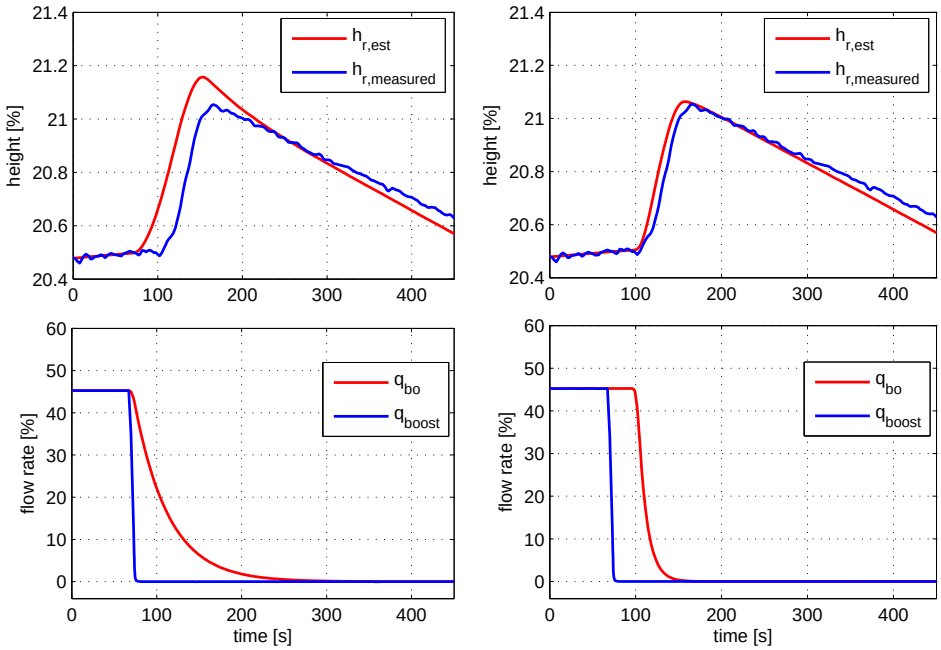

Figure 3.17: Simulation of the simplified booster pump dynamics. The upper and lower left plot shows the estimated riser level and booster flow using the first order model. The upper and lower right plot shows the estimated riser level and booster flow using the first order plus time delay model.

Ramping Up

By adding the first order plus time delay dynamics to the booster pump flow, the flow induced by the U-tubing effect for the case where the booster pump ramps down was correctly estimated. From the example calculations prior, and simulations using the tuned original model, it was estimated that the fluid level drops approximately 160 m. Refilling the booster line with a typical pump rate will take roughly 45 seconds. From this information alone, a fist order plus time delay model should fit the the ramp-up case as well. However, as mentioned there are additional uncertainty related to the booster pump flow during ramp-up. The required booster flow exceeds the calculated pump flow. To account for possible error and other effects that could cause this, a simple integrator model is suggested

$$q_{bo}(s) = \theta_i \frac{1}{s} q_{boost}(s), \qquad q_{bo} < q_{boost}^{sp} \tag{3.14}$$

with a tuning parameter, θ_i, controlling the rate of integration. The integration should stop when the estimated booster outlet flow reaches the pump set-point, denoted q_{boost}^{sp}. Figure (3.18) shows the results and the effect of θ_i. The top plot shows the estimated riser level for the different θ_i values. The bottom plot shows the corresponding estimated booster outlet flow. As seen the value for $\theta_i = 0.05$ yields the most accurate estimate. This value

was found to differ somewhat for different ramp-up cases, however to such small degree that it is considered constant.

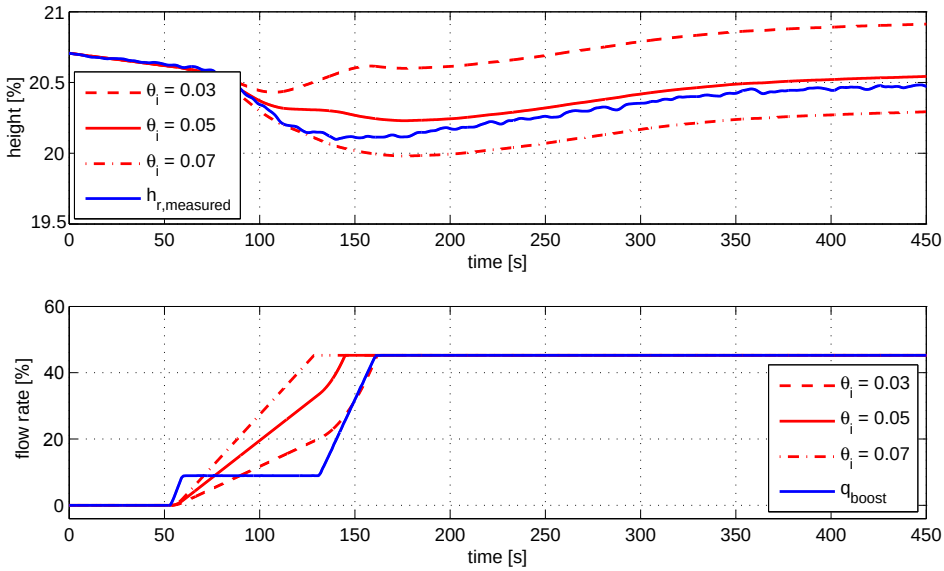

Figure 3.18: Simulation of the simplified booster pump dynamics for ramp-up using different values for the tuning parameter θ_i. The upper plot shows the estimated riser level, while the lower shows the estimated booster line flow.

Combined Model

The results using model (3.13) for ramp-down and model (3.14), with $\theta_i = 0.05$, for ramp-up is shown in figure (3.19). It is clear from inspection that the simplified booster pump dynamics manages to estimate the flow caused by U-tubing, and correct for uncertainty when ramping up. Consequently, the riser level is correctly estimated. The estimate is actually better when compared to the simulations results using the more complicated, tuned model (3.12). For the case used in this section, the estimates are very accurate. However, the model is as mentioned sensitive to tuning, and the parameter θ_i was found to vary somewhat. However, the value used above, $\theta_i = 0.05$, was found to fit most cases found in the data. The time delay and time constant,τ_d and τ_b, was found to be consistent for all U-tubing cases.

The simplified booster pump dynamics and augmented riser level dynamics are given as

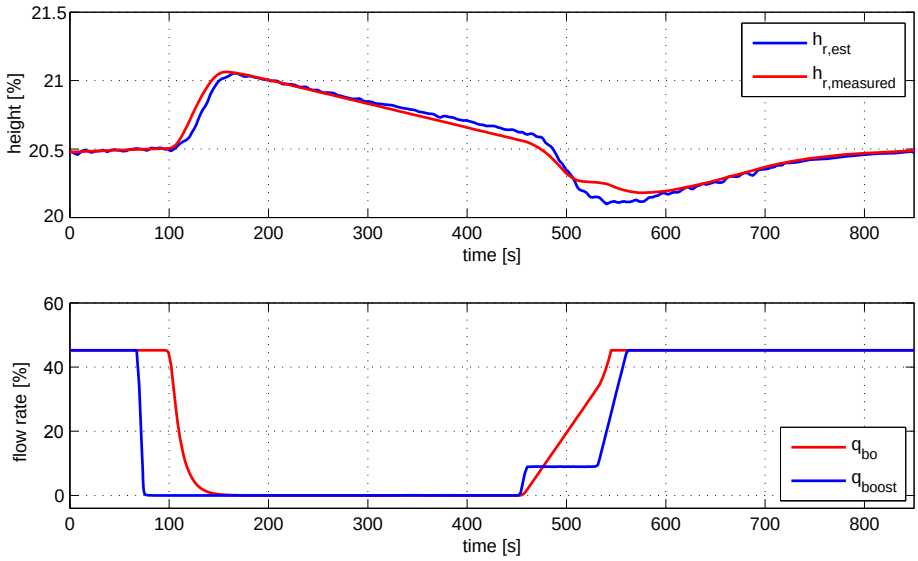

Figure 3.19: Simulation of the simplified booster pump dynamics for ramp-down and ramp-up. The upper plot shows the measured and estimated riser level. The middle plot shows the calculated pump flow and estimated booster outlet flow.

the following model

$$\dot{h}_r = \frac{1}{A_r}\left(\theta_1 q_{ssp} - q_{tf} - q_{bo}\right)$$

$$\dot{q}_{bo} = \begin{cases} \frac{1}{\tau_b}(q_{bo} - q_{boost}(t-\tau_d)), & \text{for ramp} - \text{down} \\ \\ \theta_i q_{boost}(t), & \text{for ramp} - \text{up} \end{cases}$$

3.8 Flow Dynamics

The dynamics for flow through the return line was derived in chapter 2 as

$$M_{ssp}(h_r)\dot{q}_{ssp} = p_r(h_r) + \Delta P(\omega_{ssp}, q_{ssp}) - F_r(q_{ssp}) - \rho g h_{ssp,out}.$$

Components related to friction, subsea pump, hydrostatic pressure and riser pressure are identified previously in the chapter. However, the parameter $M_{ssp}(h_r)$, which related to the transient response of the flow dynamics is yet to be identified. The theoretical value is found to be the integral of the density over the cross-sectional area of the flow section and is given as

$$M_{ssp}(h_r) = \int_{h_r}^{l_{ssp}} \frac{\rho_r(l)}{A_r(l)} dl + \int_0^{l_{ssp}} \frac{\rho_{rl}(l)}{A_{rl}(l)} dl$$

which reduces to

$$\begin{aligned} M_{ssp}(h_r) &= \frac{\rho}{A_r}(l_{ssp} - h_r) + \frac{\rho}{A_{rl}} l_{ssp} \\ &= \frac{(A_r + A_{rl})}{A_r A_{rl}} \rho l_{ssp} - \frac{\rho}{A_r} h_r \end{aligned}$$

from the fact that both the density and the cross-sectional area in the riser are constant, and not a function of depth. Inserting the true parameter values, the theoretical value for $M_{ssp}(h_r)$ is calculated as

$$M_{ssp}(h_r) = 2 \times 10^7 - 5.6 \times 10^3 h_r. \tag{3.15}$$

The riser level can not drop below the subsea pump, and thus ranges between 0 and $h_{ssp,in} = 307$ m. Consequently, the term proportional to the riser level is small compared to the constant term. It is therefore reason to assume that $M_{ssp}(h_r)$ is a constant parameter, independent of h_r. A theoretical estimate is taken as

$$M_{ssp} = 2 \times 10^7.$$

In order to further investigate M_{ssp}, and to obtain an estimate based on the available data, a recursive estimator, was designed. The estimator model is on the form

$$\hat{y}(t) = \varphi^\top(t)\theta$$

with the measurements and unknown parameter

$$\begin{aligned} y(t) &= \dot{q}_{ssp} \\ \theta^* &= \frac{1}{M_{ssp}} \\ \varphi(t) &= p_r(h_r) + \Delta P(\omega_{ssp}, q_{ssp}) - F_r(q_{ssp}) - \rho g h_{ssp,out}. \end{aligned}$$

By filtering with the simple first order filter the model becomes

$$z(t) = \phi^\top(t)\theta^*, \qquad z = \frac{y(t)}{\Lambda(s)}, \qquad \phi = \frac{\varphi(t)}{\Lambda(s)}, \qquad \Lambda(s) = \frac{1}{5s+1}.$$

The recursive estimator was implemented according to the equations in section (3.1.3), using the following design parameters

$$m = 1, \qquad \theta_{\text{init}} = \frac{1}{2 \times 10^7}, \qquad P_0 = 0.01, \qquad \beta = 0 \text{ and } 0.1$$

In order to estimate M_{ssp}, transients in flow are required as the parameter has no effect on the system for steady state conditions. An ad-hoc approach was done by extracting transients from the return line flow data and using them as input to the estimator. That is, data for q_{ssp}, and corresponding data for $p_r(h_r)$ and ω_{ssp}. The transient data is shown in figure (3.20). As seen in the second plot the variation in riser level is relatively small for

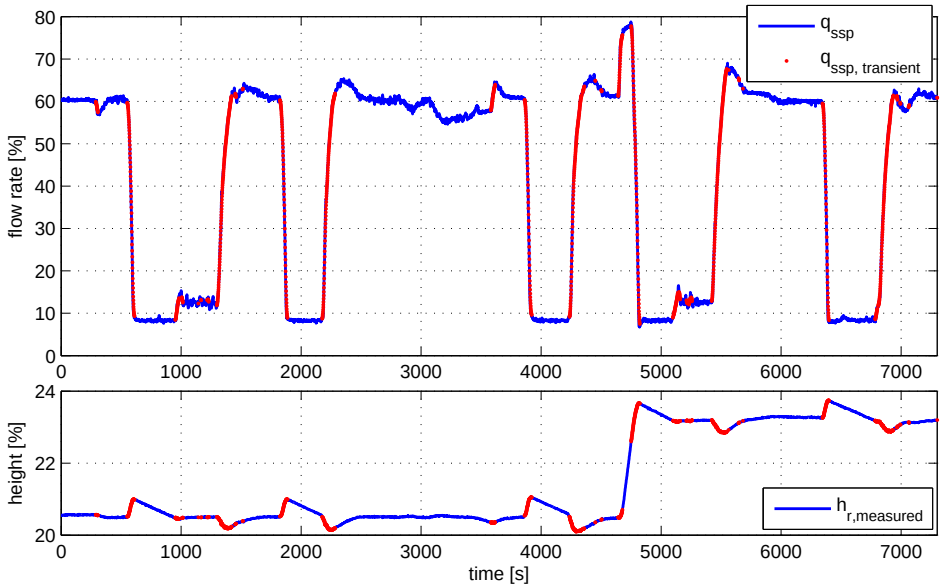

Figure 3.20: Extracted flow transients. The upper plot shows the set of measured flow rates, and the extracted transients used for the estimation. The lower plot shows the corresponding riser level.

the extracted data. This is the case for all of the available data. Consequently, a possible dependence on riser level is not expected to be possible to observe. Figure (3.21) shows the result of the estimation. The top plot shows the estimated value using pure Least- squares, that is without forgetting factor. As stated in section (3.1.3) this algorithm is guaranteed to converge as the amount of data grows. Hence, the last estimate can be interpreted as an average estimate. The second plot shows the estimated value when using a forgetting factor. In this case older data is disregarded, giving an indication of the degree of fluctuation. As seen, the estimate fluctuates, indicating that the parameter will in fact vary depending on operating conditions to some degree. This is however expected. The model itself does not capture all the aspects of the flow, only the dominating effects. Also, in addition to model error, there is uncertainty related to the previously estimated parameters. All this uncertainty will propagate to the estimate of M_{ssp}, and parameter convergence with forgetting factor is not to be expected.

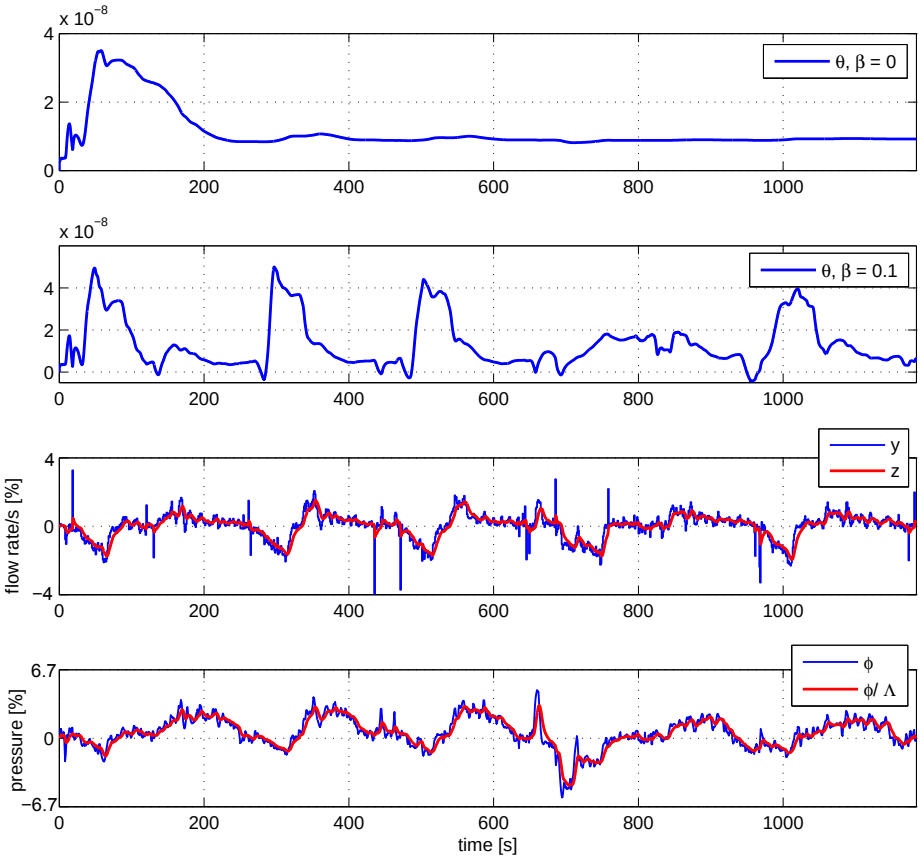

Figure 3.21: Estimated value for M_{ssp} using pure LS and LS with forgetting factor. The two upper plot show the estimated value without and with forgetting factor respectively. The two lower plots show the filtered and un-filtered measurement and regressor respectively.

Based on the estimate obtained using the pure LS algorithm, M_{ssp} is set to

$$M_{ssp} = \frac{1}{0.9 \times 10^{-8}} = 1.1 \times 10^{8}.$$

Using this value as a starting point the flow was simulated for different values of M_{ssp}, with the pump speed as input, and with the measured inlet pressure. The fourth order friction model and the pump model based on all data was used. Looking at the results in figure (3.22), it is clear that M_{ssp} is analogous to a time constant for the flow. The value estimated for M_{ssp} above results in a accurate estimate. Slight improvements is observed for a value of $M_{ssp} = 0.5 \times 10^{8}$, corresponding to even faster flow dynamics. During the simulations it was observed that multiple values below 1×10^{8} gave a satisfactory result. This shows the fact that the dynamics are incredibly fast, possibly negligible, and as long as M_{ssp} is chosen in the correct range, the flow estimate will vary to only a small degree.

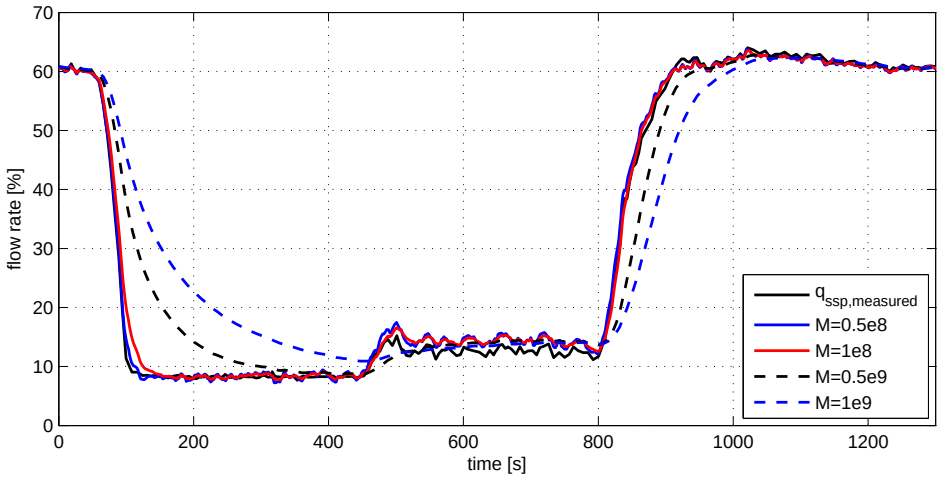

Figure 3.22: Comparison of different values for M_{ssp}.

3.8.1 Neglecting Flow Dynamics

Because of the fast flow dynamics, a possibility is to neglect the dynamics entirely, and not consider the return line flow as a state. For a given pump speed, the corresponding flow is given as a static relationship. The system then reduces to a differential algebraic equation (DAE) where the return line flow is given as the solution to the implicit equation

$$h_{\text{pump}}(\omega_{ssp}, q^*_{ssp}) = h_{\text{sys}}(q^*_{ssp}). \tag{3.16}$$

corresponding to the intersection between the system and pump curve as described in section (2.4). Inserting for the system and pump head the DAE system becomes

$$\dot{h}_r = \frac{1}{A_r}(q_{ssp} - q_{bo} - q_{tf}) \tag{3.17}$$

$$c_0\omega^k_{ssp} - c_2 q^2_{ssp} = \frac{1}{\rho g}\left(G_{\text{outlet}} - G_{\text{inlet}}(h_r) + F(q_{ssp})\right) \tag{3.18}$$

It can be discussed whether this system has any advantages compared to the original flow equation with fast dynamics. With a high order friction model, the computation of the solution to (3.16), is not necessarily straight forward. The DEA system was implemented for comparison, and the result is shown in figure (3.23). As expected, the results with and without dynamics are almost identical. For some reason the estimate without dynamics drops somewhat low at lower flow rates. However, this is a steady state problem and not related to the dynamics. In other words, the model (3.17) is a valid option.

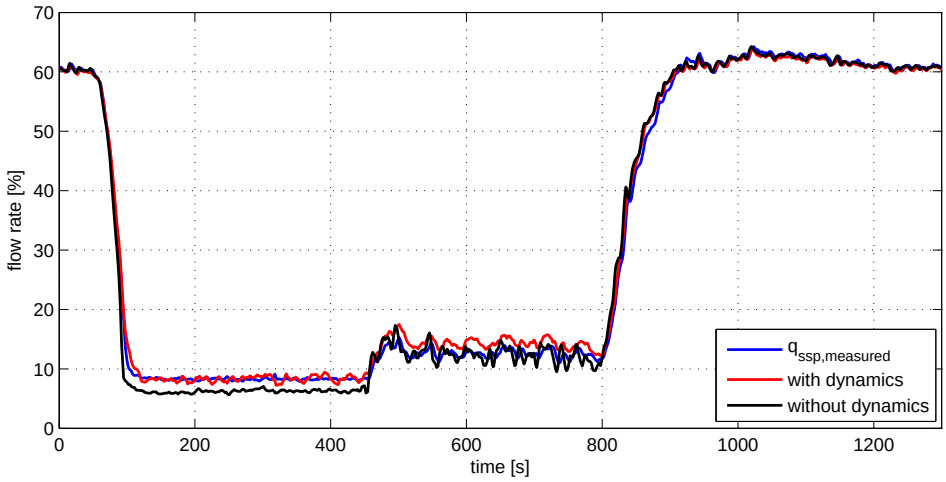

Figure 3.23: Comparison of the original flow dynamics and the static flow model.

3.8.2 Subsea pump model

From the sensitivity analysis it was found that the quality of the pump model parameters was the most crucial. From identification of the subsea pump model in section (3.5), two slightly different models were found. One based on all available data, and one based on filtered data. In order to find which of these that are most accurate in practice, simulations were done using both models. The pump speed was used as input as well as the measured inlet pressure. The result is shown in figure (3.24). ΔP_1 denotes the model based on all data, and is the model used for the flow simulations done above, and ΔP_2 denotes the one based on filtered data. ΔP_1 is clearly the superior model on a general basis. ΔP_2 is not sufficiently accurate for lower flow rates. At higher flow rates it produces slightly better estimates, however it is barely visible in the figure. The difference in accuracy for high and low flow rates are visible in the performance curves found in section (3.5), when comparing to the plotted data. But the slight gain in accuracy at high rates, obtained when using filtered data, is clearly not justified when the loss in accuracy at low rates is significant. Consequently, ΔP_1 is deemed the most accurate model.

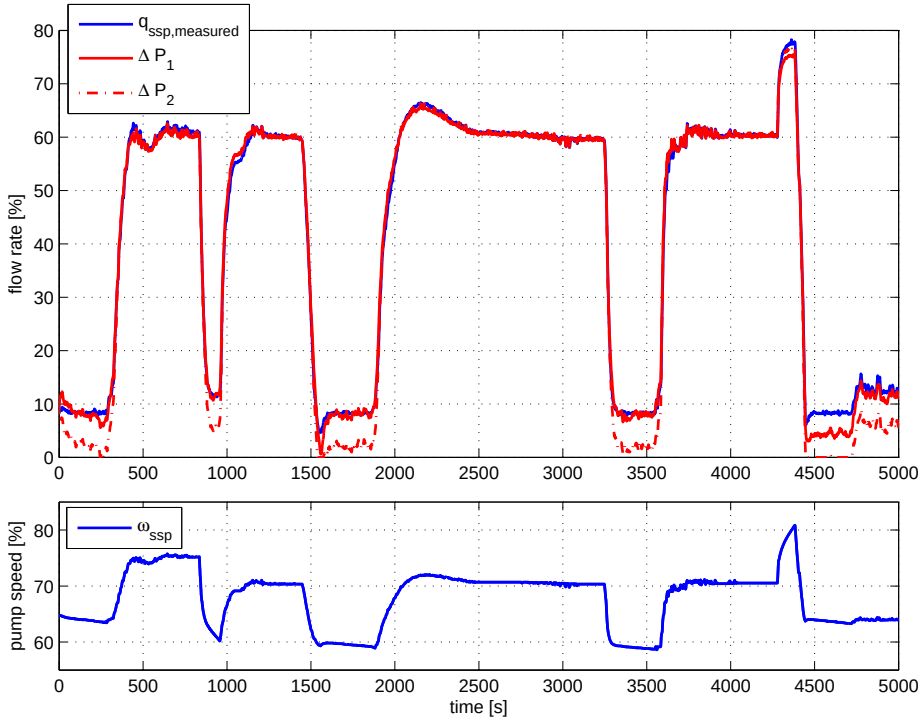

Figure 3.24: Comparison of the two identified pump models. The upper plot shows the resulted flow for the different models compared to the measured flow. The bottom plot shows the pump speed input.

Chapter 4

Model Verification

In the previous chapter the all unknown parameters have been estimated. Also, the model was revised to include the U-tubing effect. During the system identification, measurements were used as input to the different part of the system to isolate and verify the different part of the system. The ultimate goal is to be able to reproduce the measurements of the two states, using the identified model with only the pump speed, and in-flows as input. Two test cases are used to verify the model. One during normal operation conditions, where the in-flows stays at a constant rate so that no U-tubing effects are present. The other case is more comprehensive, and the comparison is done to a part of the data where the booster pump is ramped up and down multiple times. The original flow dynamics equation and the simplified U-tubing model is used.

Ultimately, the model verification should be done on completely independent data, not used previously for identification purposes. Unfortunately, this is not entirely the case. All available data was used for e.g. the friction and pump model estimation. However, this part of the data was not used for the identification for the parts related to dynamics. Hence, the verification test should give a good indication of how accurate the model is in general.

The result of the two cases is shown in figure (4.1) and (4.2) respectively. For case 1, the estimate is more or less spot on, with only a slight deviation in the riser level. This result is not surprising as both the friction and pump model has proved to be accurate. For case 2, the deviation is more evident, and clearly correlated with the occurrence of U-tubing. However, the error is not significant. The deviation in fluid level corresponds to less than 0.5 bar in riser pressure. This is e.g. in the same range as the errors found related to measurement offsets. The model manages to capture the main dynamics of the system, and with more system information and measurements related to the booster pump, an improved model for U-tubing could be obtained, which possibly could increase the accuracy. For reference, a simulation of case 2 was done without accounting for U-tubing and can be found in appendix (B) in figure (B.1).

4.1 Case 1

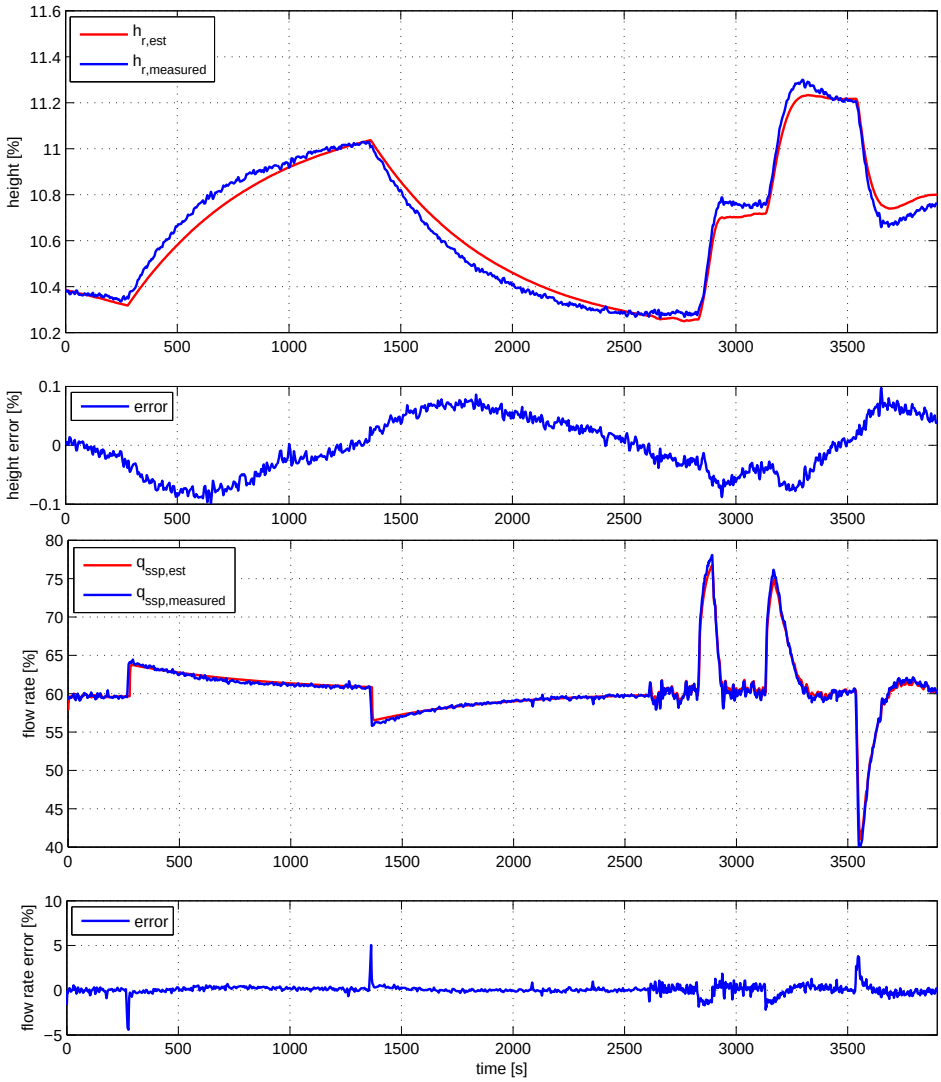

Figure 4.1: Simulation of the full system for a normal circulation case. The upper plot shows the comparison of the measured riser level and the estimated, with the error in the plot below. The third plot shows the comparison of the measured and estimated flow rate, followed by the error in the last plot.

4.2 Case 2

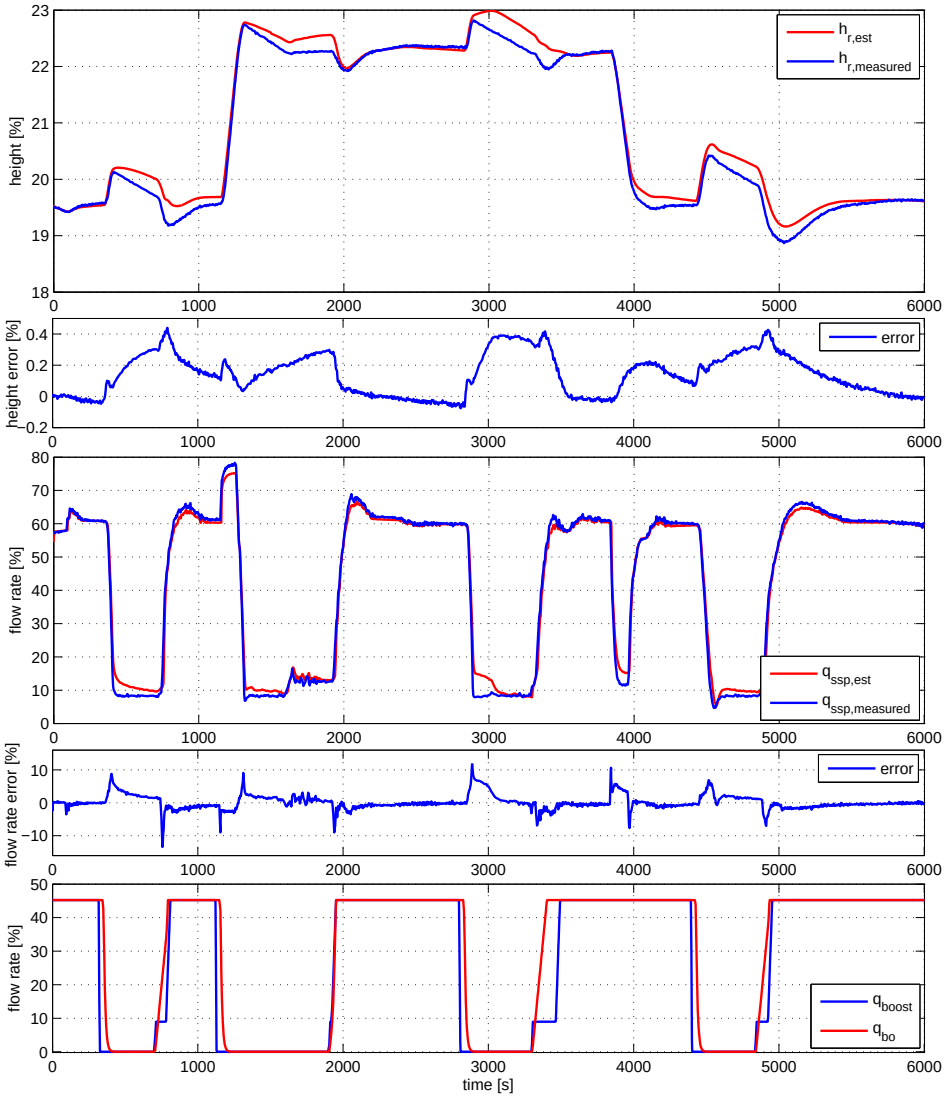

Figure 4.2: Simulation of the full system for a a comprehensive circulation case. The upper plot shows the comparison of the measured and estimated riser level, with the error in the plot below. The third plot shows the comparison of the measured and estimated flow rate, followed by the error in the blot below plot. The last plot shows the estimated booster outlet flow and calculated booster pump flow.

Chapter 5

Conclusion

A dynamic fit-for-purpose model for a dual gradient drilling system has been derived. The model was reduced to describe the mud circulation part of the system, which was the focus for the system identification part. Using field data, the unknown parameters in the model was estimated. A steady-state friction model was found sufficient to describe the frictional losses in the return line. The originally suggested model for the subsea pump was deemed inaccurate, and an improved model was obtained by optimization. A correction factor was introduced to the riser level dynamics, to correct for offset in the measurements. The presence of U-tubing was observed when ramping down the booster pump. Consequently, the level dynamics in the riser was augmented to account for the effect. However, due to the lack of measurements and in-depth system knowledge the original model was hard to validate, and relied on tuning. Hence, it was found to be inadequate. Instead, simplified dynamics was added to the booster pump, which successfully estimated the effect of U-tubing. The flow dynamics was found to be very fast. A possible model where the flow dynamics are neglected, and the return-line flow is given as a static relationship between the system and pump head, is suggested as an alternative. Lastly, the system was simulated and compared to measurements. The results showed that the derived model with the estimated parameters, and augmentations, was able to reproduce the field data in a satisfactory manner. For normal circulation, the estimate is very accurate. For a more comprehensive test case, with multiple occurrences of U-tubing the deviation from measurements is more evident and clearly correlated with U-tubing. The model does however account for the effect in a satisfactory manner.

5.1 Future Work

Because of the uncertainties related to U-tubing when the booster pump ramps down, further investigations could be done on the area. This includes obtaining in-depth information about the system the field data originates form. The uncertainties regarding pump ramp-up should be resolved in order to make the appropriate assumptions related to modeling the effect. Also, to validate a potential U-tubing model, pressure data from the pump outlet in

the booster line should be available.

An natural follow-up after the work done in this thesis is to use the presented model for control design. Various control designs i.e. model or gain-scheduling based controllers can be tested on the model. Additionally, the friction and subsea pump models estimated in this work will naturally change over time. On-line estimation schemes to contentiously update the unknown model parameters is another natural extension to be looked into.

Bibliography

Anfinsen, H., 2012. Modelling and Estimation of U-tubing Effects in the Low Riser Return System (December).

Anfinsen, H., Aamo, O. M., 2013. Disturbance rejection in 2 x 2 linear hyperbolic systems. IEEE Transactions on Automatic Control 58 (June), 1095–1106.

Breyholtz, O. y., Nygaard, G., Nikolaou, M., 2011. Managed-Pressure Drilling: Using Model Predictive Control To Improve Pressure Control for During Dual-Gradient Drilling. SPE Drilling & Completion 26 (September 2010), 4–7.

Çengel, Y., Cimbala, J., 2010. Fluid Mechanics: Fundamentals and Applications. Çengel series in engineering thermal-fluid sciences. McGraw-Hill Higher Education.

Egeland, O., Gravdahl, J., 2002. Modeling and Simulation for Automatic Control. Marine Cybernetics.

Fossum, T. O., 2013. Analysis and control of drilling riser dynamics in dual gradient drilling (June).

Godhavn, J. M., Pavlov, A., Kaasa, G. O., Rolland, N. L., 2011. Drilling seeking automatic control solutions. IFAC Proceedings Volumes (IFAC-PapersOnline) 18, 10842–10850.

Ioannou, P. A., Sun, J., 2012. Robust Adaptive Control. Prentice-Hall, Inc., Upper Saddle River, NJ, USA.

Isambourg, P., Anfinsen, B. T., Marken, C., 1996. Volumetric behavior of drilling muds at high pressure and high temperature.

Kaasa, G.-O., Stamnes, O. y., Aamo, O. M., Imsland, L., 2012. Simplified Hydraulics Model Used for Intelligent Estimation of Downhole Pressure for a Managed-Pressure-Drilling Control System. SPE Drilling & Completion 27 (March).

Kaasa, G.-O., Stamnes, O. y. N., Imsland, L. S., Aamo, O. M., 2011. Intelligent Estimation of Downhole Pressure Using a Simple Hydraulic Model. IADC/SPE Managed Pressure Drilling & Underbalanced Operations, 5–6.

Karnavas, WJ, P. J., 2009. Sensitivity Analyses of Continuous and Discrete System in the Time and Frequency Domains. Reliability, Maintainability and Safety, 2009. . . . 23 (2), 488–501.

Khalil, H., 2002. Nonlinear Systems. Prentice Hall.

Landet, I. S., 2011. Modeling and Control for Managed Pressure Drilling from Floaters.

Ljung, L. (Ed.), 1999. System Identification (2Nd Ed.): Theory for the User. Prentice Hall PTR, Upper Saddle River, NJ, USA.

Malloy, K. P., Stone, R., Medley, G., Hannegan, D. M., Coker, O., Reitsma, D., Santos, H., Kinder, J., Eck-Olsen, J., McCaskill, J., May, J., Smith, K., Sonnemann, P., 2009. Managed-Pressure Drilling: What It Is and What It Is Not. IADC/SPE Managed Pressure Drilling and Underbalanced Operations Conference & Exhibition (Figure 2).

Merritt, H., 1967. Hydraulic Control Systems. Wiley.

Smith, K. L., Gault, a. D., Witt, D. E., Weddle, C. E., 2001. SPE 71357 SubSea MudLift Drilling Joint Industry Project : Delivering Dual Gradient Drilling Technology to Industry.

Stamnes, O. N., 2011. Nonlinear Estimation with Applications to Drilling.

Stamnes, O. N., Mjaavatten, E., Falk, K., 2012. A simplified model for Multi-Fluid Dual Gradient Drilling Operations. Proceedings of the 2012 IFAC Workshop on Automatic Control in Offshore Oil and Gas Production, Norwegian University of Science and Technology, Trondheim.

Stamnes, O. y. N., Zhou, J., Kaasa, G. O., Aamo, O. M., 2008. Adaptive Observer Design for the Bottomhole Pressure of a Managed Pressure Drilling System. Proceedings of the IEEE Conference on Decision and Control, 2961–2966.

Stave, R., 2014. Implementation of Dual Gradient Drilling. In: Offshore Technology Conference. No. May. Offshore Technology Conference, pp. 5–8.

Wenaas, A., 2014. A Case Study of How MPD Techniques Can Be Used to Adapt to Uncertain Pore and Fracture Pressure Gradients (June).

White, F., 2011. Fluid Mechanics. McGraw-Hill series in mechanical engineering. McGraw Hill.

Zhou, J., Stamnes, O. y. N., Aamo, O. M., Kaasa, G.-O., 2008a. Adaptive Output Feedback Control of a Managed Pressure Drilling System (2), 1–6.

Zhou, L., Stamnes, O. N., Aamo, O. M., Kaasa, G.-O., 2008b. Adaptive Output Feedback Control of a Managed Pressure Drilling System. Proceedings of the 47th IEEE Conference on Decision and Control Cancun, Mexico, Dec. 9-11, (3908), 3008–3013.

Appendix A

System Parameters

Table A.1: System parameters and equipment locations.

Specifications	
Mud weight	1.12 sg
Riser inner diameter	19.75 inch
Drillpipe outer diameter	5 inch
Casing outer diameter	10.75 inch
Mud return line inner diameter	6.05 inch
Booster line inner diameter	6.05 inch
Pressure sensor locations	
Inlet to SPM	307 mRKB
Outlet to SPM	302 mRKB
Riser	305 mRKB
Key heights	
Booster line inlet	340 mRKB
Wellhead Datum	352 mRKB

Appendix B

Additional Plots

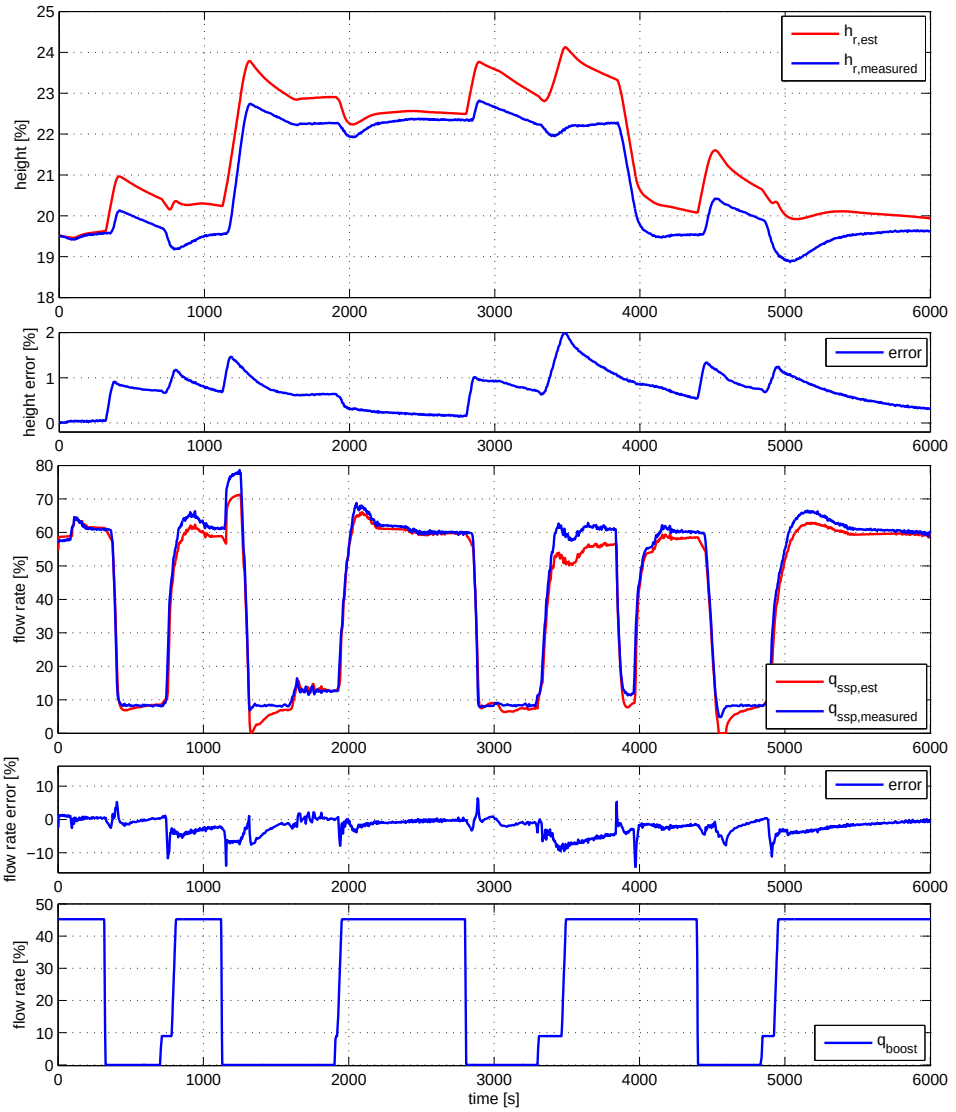

Figure B.1: Simulation of the full system for a comprehensive circulation case without accounting for U-tubing. The upper plot shows the comparison of the measured and estimated riser level, with the error in the plot below. The third plot shows the comparison of the measured and estimated flow rate, followed by the error in the blot below plot. The last plot shows the calculated booster pump flow.

Appendix C

Pump Head Derivation

Following is a short derivation of the theoretical head with reference to figure (C.1), based on White (2011), where a more detailed version is found. The assumption of one-dimensional flow (**A1**) is made and a idealized pump impeller is considered. The fluid is

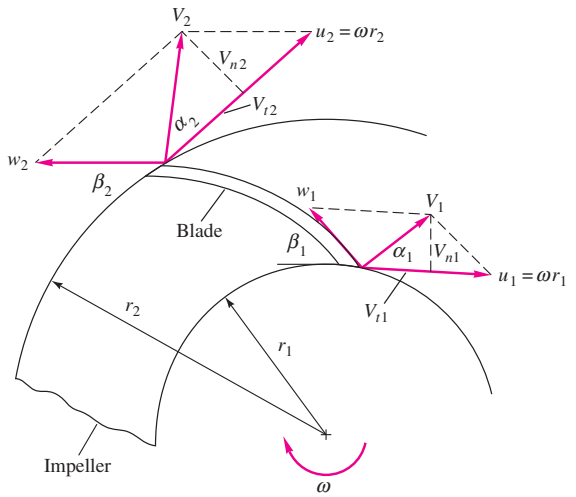

Figure C.1: Inlet and exit velocity diagrams for an idealized pump impeller. Figure from White (2011).

assumed to enter the impeller at $r = r_1$, rotating with velocity component w_1 which is tangent to the impeller blade angle β_1 plus the circumferential speed u_1. The absolute entrance velocity, V_1, is then the vector sum of w_1 and u_1. Similar, the fluid exits at $r = r_1$, with absolute velocity, V_2. The Euler equations relates ideal head and power to the pump

geometry and rotor velocities, and are given as

$$P_w = \omega T = \rho q(u_2 V_{t2} - u_1 V_{t1}) \tag{C.1}$$

$$h_{\text{pump}} = \frac{P_w}{\rho g q} \tag{C.2}$$

where P_w denotes the power delivered to the fluid, and h_{pump} is the net pump head defined as

$$h_{\text{pump}} = \frac{\Delta P}{\rho g}$$

For the case of centrifugal pumps, the power can be related to the radial velocity $V_n = V_t \tan(\alpha)$, and equation (C.1) can be rewritten as

$$P_w = \rho q(u_2 V_{n2} \cot(\alpha_2) - u_1 V_{n1} \cot(\alpha_1))$$

The inlet angular momentum can be neglected, as it is small compared to the outlet, and equation C.1 reduces to

$$P_w = \omega T = \rho q u_2 V_{n2}$$

with

$$V_{r2} = u_2 - V_{n2} \cot(\beta_2), \qquad V_{n2} = \frac{q}{2\pi r_2 b_2}$$

where b_2 is the blade width at the exit. Consequently, he theoretical head becomes

$$h_{pump} = \frac{1}{g} u_2^2 - \frac{\cot(\beta_2)}{2\pi r_2 b_2 g} u_2 q$$

Substituting u_2 with the rotational velocity, ω, the theoretical head in terms of flow rate and pump speed is given as

$$h_{pump} = \frac{r_2^2}{g} \omega^2 - \frac{\cot(\beta_2)}{2\pi b_2 g} \omega q. \tag{C.3}$$